ELSEVIER

Precambrian Research 120 (2003) 149–175

Precambrian Research

www.elsevier.com/locate/precamres

The Proterozoic Hustad igneous complex: a low strain enclave with a key to the history of the Western Gneiss Region of Norway

Håkon Austrheim [a,*], Fernando Corfu [b,1], Inge Bryhni [b,2], Torgeir B. Andersen [a,3]

[a] *Department of Geology, University of Oslo, P.O. Box 1047, Blindern, 0316 Oslo, Norway*
[b] *Geological Museum, PB 1172, Blindern, 0318 Oslo, Norway*

Accepted 18 October 2002

Abstract

The Hustad Igneous Complex (HIC) is a concentrically zoned, high K calc-alkaline intrusive complex, with a core of quartz–monzonite and granite surrounded successively by monzodiorite and pyroxenite, preserved in a 10 km^2 lens within the strongly 'caledonised' Western Gneiss Region (WGR) of Norway. Upper intercept U–Pb zircon ages of 1654±1 and 1653±2 Ma, obtained from the granite and the monzodiorite, respectively, overlap with a Rb–Sr whole rock age of 1656±49 Ma (I.R.: 0.70193±0.0009, MSWD:6.6) obtained from the felsic members of the complex and a Sm–Nd whole rock age of 1555±180 Ma (I.R.: 0.51067±13, MSWD:3.3). The U–Pb age of 1654±1 Ma is interpreted to date the time of intrusion. A 50 m thick dolerite dyke that can be followed for almost 4 km across the HIC yields a U–Pb zircon and baddeleyite age of 1251±3 Ma. The dyke also contains a secondary polycrystalline zircon generation, which together with baddeleyite defines a lower intercept age of 384±9 Ma. The Caledonian events were also marked by the emplacement of a swarm of pegmatites, which crosscut all the other units and provide a U–Pb zircon age of 401±1 Ma. A Rb–Sr whole-rock age for the pegmatites is older at 452±26 Ma (I.R.: 0.7105, MSWD:4.3) indicating some initial isotopic heterogenity and formation of the pegmatites from material with a long crustal residence time. A concordant U–Pb monazite age of 390±2 Ma from the pegmatite and the above 384±9 Ma lower intercept age date metamorphism caused by percolating fluids. Post pegmatite deformation transformed the complex along shear zones into gneisses indiscernible from the surrounding gneisses. The HIC is characterised by high mg-numbers (0.39–0.80), high Ni and Cr values, and depletion of Nb and Ta relative to LIL elements. Phenocrysts of ortho- and clinopyroxene have high concentrations of Cr, supporting the Cr-rich nature of the complex. The suite is LREE-enriched, has a fractionated and U- shaped REE pattern (Ce_n 90–143, Yb_n 12–40), e_{Nd} values ranging from +0.0 to +2.7, and the

* Corresponding author. Fax: +47-22-85-4215
E-mail addresses: hakon.austrheim@geologi.uio.no (H. Austrheim), fernando.corfu@nhm.uio.no (F. Corfu), inge.bryhni@nhm.uio.no (I. Bryhni), t.b.andersen@geologi.uio.no (T.B. Andersen).
[1] Fax: +47-22-85-1800.
[2] Fax: +47-22-85-1800.
[3] Fax: +47-22-85-4215.

PII: S0301-9268(02)00167-5

felsic members display weak positive Eu anomalies while the pyroxenite has a negative Eu anomaly. The complex bears a geochemical resemblance to the late-tectonic, high-Ba–Sr granite complexes of West Scotland, and particularly to their volcanic counterparts, the Mg-rich Old Red Sandstone andesites. Overall the data suggest generation of the suite in a subduction environment from material derived by melting of a recently enriched, but previously long-term LREE-depleted mantle. The HIC is one of the few well-preserved remnants of the igneous protoliths of the 1686–1640 Ma gneisses that make up the WGR. In fact, the pyroxenite is compositionally identical to orthopyroxene eclogite found as lenses in the surrounding gneisses and forms a likely protolith to this enigmatic rock. The metamorphism had little influence on the Rb–Sr and Sm–Nd systems of the felsic rocks, but it appears to have affected more strongly those in the mafic rocks, probably as a result of the more intense mineralogical transformations and metasomatic loss of Rb and LREE during high-grade metamorphism.

Keywords: Western Gneiss Region, Norway; Proterozoic; Caledonian; U–Pb; Sm–Nd; Rb–Sr isotope geology; Magmatism

1. Introduction

Gneiss-terrains constitute a major part of the continental crust and in shield areas they make up more than 50% of the total exposures. These terrains may have obtained their gneissic structure and metamorphic character during orogenic events that followed shortly after their formation or they may have suffered reworking during one or several later events. Our limited knowledge about the formation and geochemical evolution of these large areas of gneiss is a major obstacle to a better understanding of continental growth. The discovery of coesite and diamonds (Chopin, 1984; Smith, 1984; Dobrzhinetskaya et al., 1995) in some of these gneiss domains demonstrate that they have been subducted to depth of over 100 km, where they may have interacted geochemically with the upper mantle. The metamorphic transitions that occur under such conditions have been well documented and it has been demonstrated that high P metamorphism was aided and driven by a fluid phase. However, we know little about the role of this fluid phase in large-scale geochemical transport. It seems as a paradox that while metasomatism of the mantle wedge is well documented, such a process is hardly ever evaluated when discussing the geochemical signature of gneiss terrains. In order to resolve the chemical effect of fluid driven metamorphism we must be able to distinguish the chemical characteristics of primary magmatic processes from the fluid-induced metamorphic and metasomatic processes. In gneiss terrains this is difficult since the original mineralogy and structure were destroyed during deformation. Fortunately, the strain pattern in reworked terrains is inhomogeneous, in such a way that strain is taken up in zones varying from meter-thick shear zones to mobile belts tens of kilometres across, leaving lenses of undisturbed and less altered rocks behind. This relationship provides a mean to look through later deformation and metamorphism into the earlier history of the gneisses.

The Western Gneiss Region (WGR) of Norway refers to a more than 25 000 km^2 area of dominantly gneissic rocks outcropping between Bergen and Trondheim (Fig. 1). This large basement window is overlain by a series of Caledonian Nappes and, with some exceptions, is equivalent in terms of age to the gneisses of Vestranden north of the Trondheimsfjord (Fig. 1). Ages in the range 1700–1600 Ma have been obtained throughout the area suggesting that large proportions of the crust formed at that time followed by subsequent emplacement of minor anorthositic and gabbroic rocks, rapakivi granites and mangeritic bodies between 1520 and 1250 Ma (Table 1 and Fig. 1). The southern areas of the WGR underwent Sveconorwegian activity in form of granite intrusions and migmatites (e.g. Skår and Pedersen, 1998; Tucker et al., 1990), and were then affected by a high to medium grade metamorphic event at approximately 395 Ma during the Caledonian orogeny (e.g. Tucker et al., 1986/1987). The WGR forms part of the Baltic Shield, which according to Gorbatschev and Gaal (1987) grew during 4 orogenies between 3.5 and 1.5 Ga

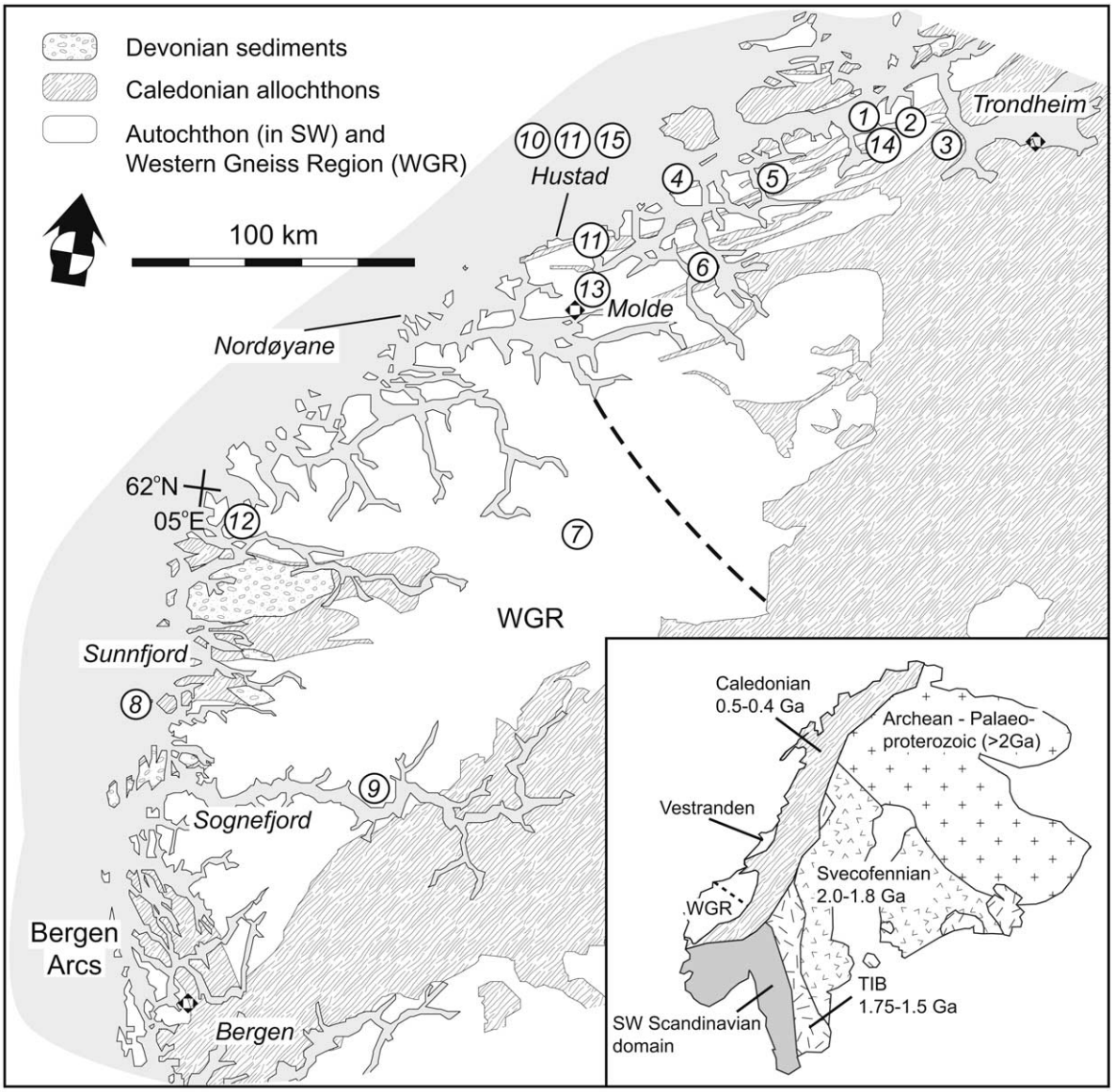

Fig. 1. Map of the WGR with the location of the ages quoted in Table 1 (encircled numbers). The dotted line defines the northern limit of the domain affected by the Sveconorwegian orogeny (after Tucker et al., 1990). Inset map showing the main subdivisions of the Baltic Shield: the Archean core, the Svecofennian Province, the Transscandinavian Igneous Belt (TIB), the Sveconorwegian SW-Scandinavian domain, and the WGR and Vestranden.

followed by reworking during Sveconorwegian (1.2 and 0.9) and Caledonian (400 Ma) events. These authors include the WGR in the Gothian belt, which developed between 1.75 and 1.55 Ga, and correlate the WGR with the Southwest Scandinavian Domain (Fig. 1). Tucker et al. (1990) suggest that the Sveconorwegian influence was limited to the southern part of the WGR as shown in Fig. 1.

The WGR is a classical area for high-pressure rocks and is known for garnet peridotites and the numerous pods and lenses of mafic eclogite,

Table 1
U–Pb zircon protolith ages from the WGR, Norway

	Rock type	Locality	Region	Age	Reference
Gothian					
1	Leucogabbro gneiss	Damvatn	Sør-Trøndelag	1657 +5/−3	Tucker et al., 1990
2	Granitic gneiss	Sagfjord	Sør-Trøndelag	1661 ±2	Tucker et al., 1990
3	Granite gneiss	Ingdal	Sør-Trøndelag	1653 ±2	Tucker et al., 1990
4	Granite gneiss	Frei	Sør-Trøndelag	1658 ±2	Tucker et al., 1990
5	Migmatite gneiss	Åstfjord	Sør-Trøndelag	1659 ±2	Tucker et al., 1990
6	Migmatite gneiss	Tingvoll	Nordmøre	1686 ±2	Tucker et al., 1990
7	Migmatite gneiss	Breidalsvatn	Nordfjord	1662 +41/−29	Tucker et al., 1990
8	Quartz diorite	Atløy	Sunnfjord	1641 ±2	Skår et al., 1994
9	Gneiss and migmatite	Kvamsøy	Sognefjord	1631 ±9	Skår, 2000
10	Granite	Hustad	Romsdal	1654 ±1	This work
11	Monzodiorite	Hustad	Romsdal	1653 ±2	This work
Post Gothian					
12	Syenite	Flatraket	Nordfjord	1520 ±20	Lappin et al., 1979
13	Granitic gneiss	Molde	Romsdal	1508 ±10	Tucker et al., 1990
14	Coronitic gabbro	Selnes	Sør-Trøndelag	1462 ±2	Tucker et al., 1990
15	Coronitic gabbro	Hustad	Romsdal	1251 ±3	This work

varying in size from decimetres up to several hundred metres across, typically embedded in amphibolite-facies gneisses. There existed a gradient with temperatures and pressures ranging between 600 °C and 12 kbar inland to 750–800 °C and over 20–28 kbar in the outer coastal area (Krogh, 1977; Smith, 1984). These extreme pressures and intense deformation were obtained when part of the WGR formed the deep root to the Himalayan-like mountain range developed during collision between Baltica and Laurentia in Caledonian time (Austrheim and Mørk, 1988; Andersen et al., 1991).

Previous work in the WGR has been focused mainly on the petrology of the eclogites, garnet peridotites and associated pyroxenites while comparatively little attention has been paid to the volumetrically dominant quartzofeldspatic ortho- and paragneisses. In this paper we describe an igneous complex found in a low strain domain in the northern part of the WGR (Fig. 1). We present U–Pb, Rb–Sr and Sm–Nd isotopic data, mineral chemistry as well as major and trace element compositions of the various rock types studied in an attempt to date and to place what may be one of the few preserved remnants of the precursors to large volumes of the WGR into a geotectonic classification. We also briefly outline the influence of the deep Caledonian subduction on this magmatic complex.

2. Field relationships

The Hustad Igneous Complex (HIC) is situated on the coast at Hustad northwest of Molde in the core of the WGR of Norway (Fig. 1). Hernes (1956) described the area and mentioned the presence of dolerites. The complex has a roughly circular form and covers approximately 5 km^2 on land but the same rock types outcrop on several small islands to the west (Fig. 2) suggesting that the HIC has a minimum areal extent of 10 km^2. The Hustad complex is intruded by a dolerite dyke and both are in turn cut by numerous pegamatite dykes.

The different rock types of the Hustad complex have a concentric distribution with a leucocratic core dominated by granite and quartz-monzonites, surrounded by a several 100 m wide zone of dark coloured monzodiorite. The monzodiorite locally displays rhythmic layering and in places contains abundant xenoliths of quartz monzonite. Locally the amount of quartz and feldspar increases and

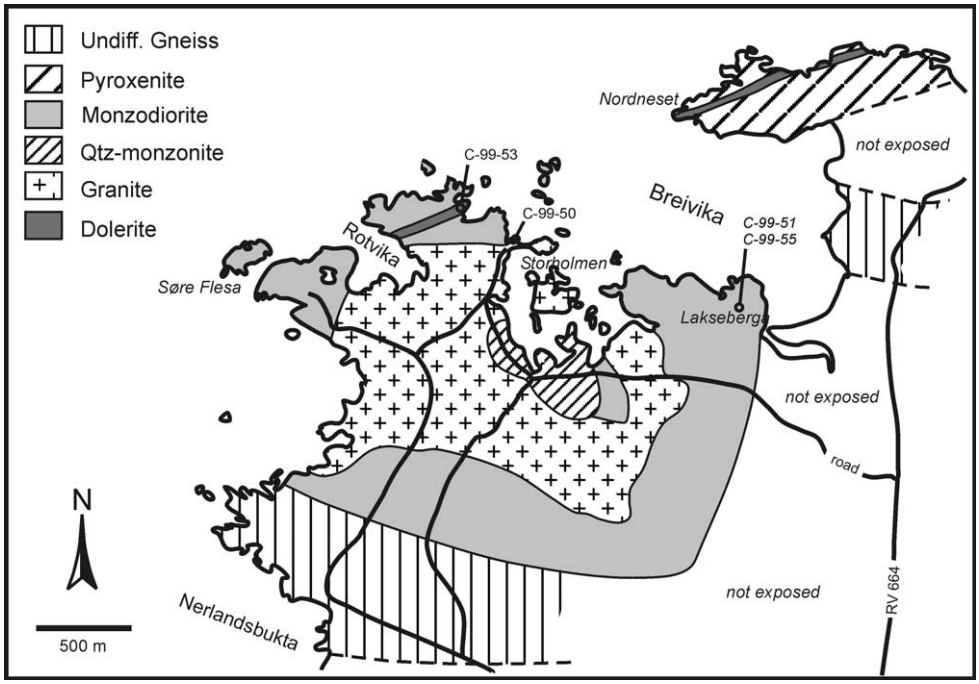

Fig. 2. Map of the HIC with sampling localities for U–Pb geochronology.

the monzodiorite grades into quartz-monzonite. In hand-specimen euhedral pyroxene and lath shaped plagioclase grains can be seen, clearly demonstrating its igneous origin. The granite is intruded by monzodiorite and quartz-monzonite.

On its northern side the complex is bordered by a 500 m wide zone of pyroxenite transitional into melagabbro. This unit shows rhythmic layering defined by varying amounts of plagioclase. Locally the layering shows channel- and cross-bedding structures (Fig. 3a). Xenoliths are widespread and at the lighthouse on Nordneset they become so abundant that the rock develops into an intrusive breccia. The xenoliths have a mafic character and range from massive to well banded. The massive type has relict igneous textures and may represent deeper cumulates of the HIC. Well-banded rocks, where the banding is defined by variations in modal amounts of amphibole, garnet, pyroxene, plagioclase and scapolite with minor quartz, may represent the wall rock to the HIC or xenoliths of the crust through which the magma passed. However, the minerals that define the banding are co-facial with those formed during the Caledonian metamorphism, and the possibility exists that they represent progressive scapolitisation and metamorphism of the gabbroic xenoliths.

The HIC is intruded by a 50–100 m thick dolerite dyke, which can be followed continuously for 1 km along the peninsula Nordneset. An identical dyke occurs on the other side of the bay (Breivika) in the continuation of the dyke on Nordneset, suggesting that they are part of a more than 4 km long dyke. The form of this dolerite contrasts with the numerous highly disrupted lenses and boudins of dolerite found in the migmatitic gneisses over most of the WGR. It demonstrates that this complex is a low strain area and that the many and variably eclogitised dolerite lenses may represent broken up fragments of former regional dolerite dyke swarms.

Pegmatites cut all members of the complex and the dolerite. On the small island of Søre Flesa (Fig. 2) one dyke can be followed for 100 m. The least deformed pegmatites are clearly dilational dykes, commonly 0.1–0.5 m wide and locally forming swarms spaced at 1.5–5 m intervals. They have a preferred orientation, striking between NW and N,

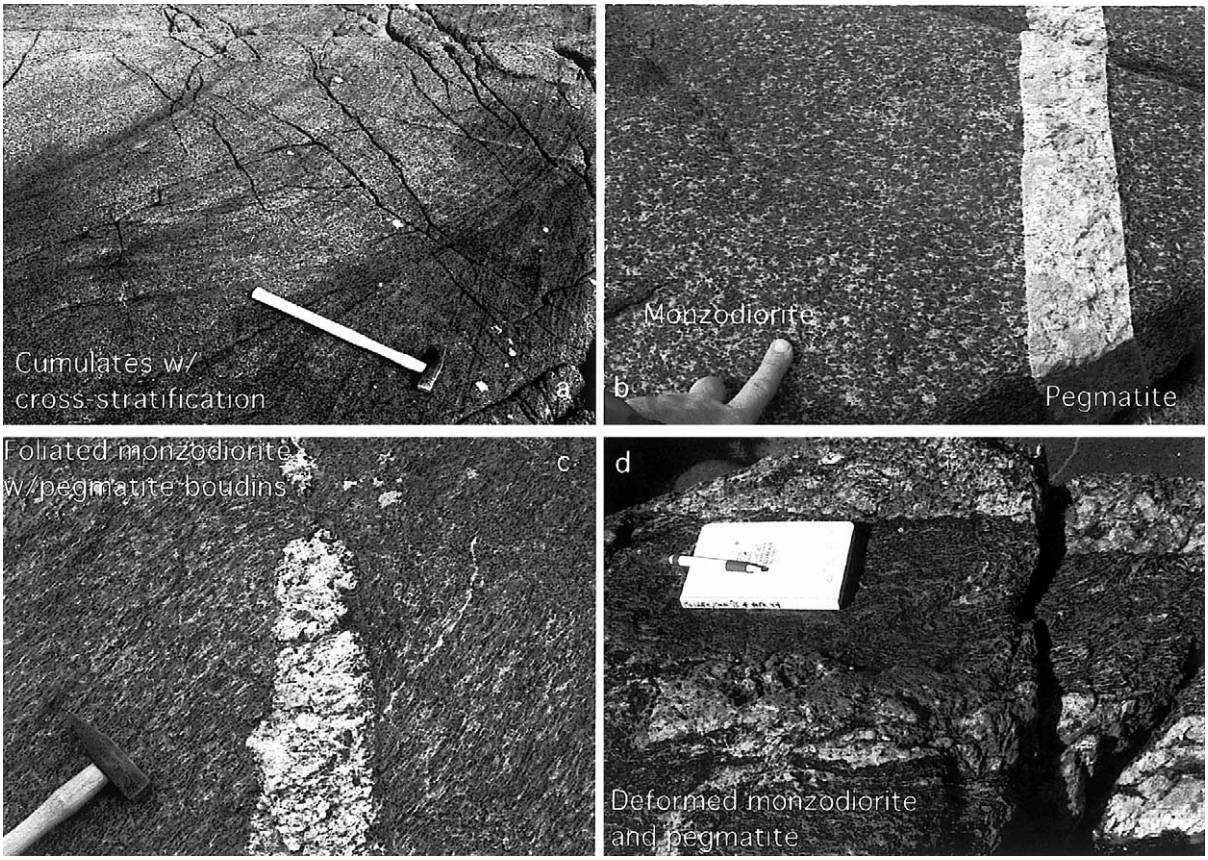

Fig. 3. (a) Exceptionally well-preserved primary magmatic structures with cross bedded cumulates in pyroxenites at Nordneset. Hammershaft is 0.5 m long. (b) Vaguely banded monzodiorite cut by late Caledonian granite pegmatite. Notice the sharp, straight margins and the undeformed nature of the dilational pegmatite dyke. From the dating locality at Lakseberga (see Fig. 2). (c) Foliated and boudinaged monzodiorite and granite pegmatite. The field relationships south of Rotvika (Fig. 2) provide a complete transition of nearly undeformed igneous rocks to their gneissic counterparts. In this photo the intrusive relationship may still be discerned. (d) Highly deformed banded gneiss formed in a local shear zone affecting the monzodiorite and the late granite pegmatite. Locality near dated rock at Lakseberga (Fig. 2).

are steep and have straight contacts (Fig. 3b), and were apparently emplaced at a high angle to the regional stretching lineation of the area. Some taper out laterally and reappear in an en echelon fashion. There was no foliation development in the HIC prior to the intrusion of the pegmatite.

The HIC is surrounded by gneisses, which range in composition from granitic to gabbroic (locally ultramafic) and exhibit a strong NE-trending foliation and a shallow plunging lineation. The mafic parts are found as lenses of retrograde eclogites, which can locally be shown to have developed from former dolerite intrusions. The change in compositions may occur on various scales, from that defined by centimetre-size banding to that of kilometre-sized bodies of foliated but homogeneous rocks, exemplified by the Dråga gneiss, which can be followed as a 500 m thick zone of granodioritic composition for 10 km along strike (Bryhni et al., 1988). The gneisses are frequently developed as migmatites, with coarse, pink or red neosome in places cutting through the gneissic banding. The gneissic banding is defined by alternating amphibole- and feldspar-rich lithologies. Towards the border of the complex and along shear zones, which tend to be concentrated

along the dykes, the pegmatites are folded and broken up and the wall rock becomes gneissic (Fig. 3c and d). In such places the HIC rocks can no longer be distinguished from the surrounding migmatite gneisses. The southern border of the complex is gradational into the gneisses. These observations suggest that igneous complexes like the one described here may have been the protolith to large part of the northern WGR.

3. Petrography

The rocks of the HIC show all stages of transformation of magmatic into metamorphic mineralogy. This transition is complete in the sheared parts, but in the less deformed parts the igneous mineralogy is partially preserved, although all parts of the complex shows sign of alteration in the form of coronas. These reactions were strongest in the pyroxenite and the xenoliths. In spite of this later metamorphism it is possible to identify and in places to analyse the primary phases.

Primary minerals in the *pyroxenite* are orthopyroxene, diopside, hornblende and minor plagioclase. The primary pyroxenes are euhedral and the clinopyroxene displays exolution lamellae. Plagioclase is recrystallised into a fine-grained aggregate, but the outline of the original grains can be traced from the extinction of the aggregate, defining a sub-ophitic texture. Secondary minerals involve garnet, clinopyroxene2, orthopyroxene2, hornblende2, and scapolite. Sulfides, including pentlandite, chalcopyrite, bornite and pyrite, are present as accessory phases. The massive xenoliths contain the same minerals as the pyroxenite, but in most samples the orthopyroxene is recrystallised and surrounded by garnet coronas.

The *monzodiorite* crystallised as an assemblage of orthopyroxene, clinopyroxene, plagioclase, *K*-feldspar and quartz. Under the microscope the lath-shaped outline of plagioclase, seen in hand-specimen, appears as a mosaic of small plagioclase grains with numerous inclusions of biotite. Clinopyroxene is optically zoned with dark dusty zones, which reflect exsolution of numerous Cr-bearing magnetite grains. Both pyroxenes contain inclusions of apatite, which are locally associated with minute monazite grains. K-feldspar also occurs in fine granular aggregates often together with quartz. Secondary minerals are, hornblende, scapolite and garnet. Biotite occurs both as a primary phase (inclusions in zircons) and as a secondary phase in recrystallised feldspar aggregates (see above). Biotite and amphibole also form in crude corona-fashion surrounding pyroxene. In the strongly altered equivalent, hornblende with inclusions of quartz completely replaces pyroxene.

The *granite* is pink, medium-grained and homogeneous without obvious foliation. It can be classified as a monzogranite composed of alkali-feldspar (microcline with characteristic twin pattern and sometimes developed as microperthite), plagioclase (locally saussuritised), quartz, biotite (olive green/yellow pleochroism and with inclusions of sphene and zircon), and minor amphibole, pale mica (as sericite in altered plagioclase and as parallel intergrowths in biotite), magnetite, apatite and orthite. The *quartz-monzonite* carries the same minerals as the granite but with a higher relative abundance of plagioclase and hornblende.

The dolerite dyke is medium-grained and in most places it has preserved its sub-ophitic texture with clinopyroxene partly surrounding lath-shaped plagioclase. The latter is extensively replaced by garnet. Fe–Ti oxides are surrounded by biotite and garnet. Aggregates of orthopyroxene surrounded by clinopyroxene, plagioclase and garnets have formed from magmatic orthopyroxene or olivine through reaction with plagioclase. The extensive corona growth of garnet between plagioclase and primary clinopyroxene, Fe–Ti oxides and olivine/orthopyroxene has led to typical honeycomb (fishnet) textures similar to those described by Mørk (1985) from Flemsøy, Nordøyane (Fig. 1).

The main constituents of the *pegmatites* are quartz, a brick-red alkalifeldspar (Or_{95}), plagioclase ($Ab_{70}An_{24}Or_6$) and minor biotite with traces of carbonates. Quartz typically forms interstitially to plagioclase. The pegmatites are variably altered. Secondary minerals including calcite, sericite and veins of euclase ($BeAl(OH)SiO_4$) surrounded by K-feldspar. The alteration typically forms around fractures and may be related to percolating fluid

emanating from a late Caledonian regional fracture system.

4. Cr-rich composition of pyroxenes

Mineral compositions of primary pyroxenes were analysed with a Cameca Camebax microprobe at the Geological museum, Oslo. The analyses were performed by wavelength dispersive spectrometry, and data reduction was carried out with a Cameca PAP software package. Natural minerals and synthetic phases were used as standards. The analyses were performed by rastering the beam to average exolution lamellae and host pyroxene. Compositions of pyroxenes are listed in Table 2.

The gabbro xenoliths and the pyroxenites contain the most primitive pyroxenes in terms of Mg/Fe ratio; they classify as diopside and bronzite. The clinopyroxenes in the monzodiorite are augites. The clinopyroxene shows zonation in the form of 10–20 μm thick zones with abundant exolution of Cr-rich magnetite and Cr-bearing ilmenite. These zones contain up to 1 wt.% Cr_2O_3 (Table 2). Orthopyroxene in the pyroxenite is around En76 and contains up to 0.9 wt.% Cr_2O_3. In sample FAR45A ortho- and clinopyroxene both contain the same high amount of Cr_2O_3 (Table 2). Similar clinopyroxene compositions with 0.6 and 1.2 wt.% Cr_2O_3, have been reported by Fortey et al. (1994), Fowler and Henney (1996) from the appinitic intrusions in the Lake District (UK) and Scottish Highland, respectively. The moderate contents of Al and Ti in the HIC pyroxenes (Table 2) are distinct from those observed in alkali basalts.

5. U–Pb geochronology

5.1. Analytical procedure

The analysed minerals were extracted from rock samples weighing approximately 2–4 kg by crushing and pulverizing in a jaw crusher and a hammer mill and various steps of enrichment using Wilfley table, Frantz separator and heavy liquids. They were handpicked in alcohol under a binocular microscope. Most zircons and one baddeleyite fraction were abraded (Krogh, 1982) prior to dissolution. The ID-TIMS procedure was done according to standard techniques (Krogh, 1973) as described for this lab in Corfu and Evins (2002). All the minerals were dissolved in teflon bombs at 184 °C, except for monazite that was dissolved in Savillex vials. Ilmenite was processed with a two-stage HBr–HCl–HNO_3 procedure. The analyses were corrected for blanks of ≤ 2 pg Pb and 0.1 pg U. The residual common Pb was subtracted using compositions estimated with the Stacey and Kramers (1975) model. The uncertainties on the ratios are given as 2σ values and were estimated by quadratic propagation of the main sources of error, including reproducibility terms of $\pm 0.05\%$ per amu for static, and $\pm 0.1\%$ per amu for S.E.M. measurements. The results are plotted using the program ISOPLOT (Ludwig, 1999).

6. Sample characteristics and results

6.1. Monzodiorite (C-99-50)

The zircon population in the monzodiorite sample ranges in shape from well preserved euhedral prismatic crystals to strongly subrounded grains. The most prominent feature are the numerous and large inclusions of other minerals, and probably melt, that also result in generally very irregular external surfaces. Thus, even after abrasion it was difficult to find grains for analysis that were entirely free of inclusions. The four zircon analyses yield relatively high U-content close to 500 ppm, relatively high but variable Th/U ratios of 0.6–1.3, and they plot 2.2–4.5% discordantly (Table 3 and Fig. 4a). Coexisting monazite occurs as a heterogeneous population of grains that generally have dark-brown cores surrounded by lighter rims. Two pairs of analyses were carried out on the two extremes using uniformly light and dark grains, respectively. The results indicate a considerable variation in terms of U contents and Th/U ratios, whereby there is a positive correlation between the U and the Th contents (Table 3), but no correlation between these properties and the

Table 2
Composition of pyroxenes from the Hustad complex

	Clinopyroxene									Orthopyroxene			
Sample	FAR14	FAR14	FAR14	FAR14	FAR31	FAR31	FAR45A	FAR45A	IB84-65	T9	FAR31	FAR45A	FAR46A
Core/Rim	Core	IZ	BIZ	IZ	IZ	Core	Core	Rim	Core	Core	Core	Core	Core
Rock type	MD	MD	MD	MD	MD	MD	PX	PX	XEN	DO	MD	PX	PX
SiO_2	52.31	51.69	53.46	50.28	50.61	50.76	52.99	53.38	53.07	51.52	52.26	54.51	54.09
TiO_2	0.16	0.20	0.08	0.89	0.17	0.42	0.30	0.23	0.41	1.27	0.08	0.11	0.09
Al_2O_3	2.44	1.72	1.56	1.97	1.73	2.71	2.41	2.74	2.71	5.11	1.36	2.19	2.44
FeO	9.04	10.39	8.62	11.67	11.27	10.13	5.54	5.90	3.91	6.95	21.45	13.57	13.31
MnO	0.16	0.16	0.22	0.15	0.11	0.20	0.19	0.17	0.09	0.04	0.39	0.28	0.38
MgO	13.01	13.39	13.69	12.47	13.18	13.10	15.87	16.24	15.59	12.24	22.51	27.14	27.04
CaO	20.81	20.21	21.03	20.74	21.35	20.30	21.76	21.61	23.78	21.00	1.79	1.19	1.42
Na_2O	1.43	1.35	1.29	1.44	1.19	1.33	0.63	0.58	0.67	2.14	0.05	0.05	0.05
K_2O	0.19	0.04	0.02	0.01	0.02	0.31	0.03	0.05	0.03	0.04	0.00	0.01	0.00
Cr_2O_3	0.19	0.77	0.33	0.91	0.76	0.31	0.49	0.16	0.12	0.15	0.00	0.51	0.87
Total	99.74	99.92	100.30	100.54	100.39	99.55	100.19	101.06	100.38	100.46	99.90	99.56	99.69
Structural formulae based on 6 (O) and 4 cations													
Si	1.944	1.921	1.971	1.869	1.877	1.897	1.935	1.932	1.929	1.884	1.940	1.962	1.944
AlIV	0.042	0.054	0.017	0.096	0.084	0.080	0.057	0.061	0.063	0.101	0.050	0.042	0.057
AlVI	0.065	0.022	0.050	−0.009	−0.009	0.040	0.047	0.056	0.053	0.119	0.009	0.051	0.047
Ti	0.005	0.006	0.002	0.025	0.005	0.012	0.008	0.006	0.011	0.035	0.002	0.003	0.002
Fe^{3+}	0.086	0.151	0.073	0.210	0.230	0.139	0.045	0.042	0.049	0.090	0.060	−0.027	−0.003
Cr^{3+}	0.006	0.026	0.011	0.031	0.026	0.011	0.017	0.006	0.004	0.005	0.000	0.019	0.032
Fe^{2+}	0.194	0.172	0.192	0.153	0.119	0.178	0.124	0.137	0.070	0.123	0.605	0.435	0.403
Mn	0.005	0.005	0.007	0.005	0.003	0.006	0.006	0.005	0.003	0.001	0.012	0.009	0.011
Mg	0.721	0.742	0.752	0.691	0.729	0.730	0.864	0.876	0.845	0.667	1.246	1.456	1.449
Ca	0.828	0.805	0.831	0.826	0.849	0.813	0.851	0.838	0.926	0.823	0.071	0.046	0.055
Na	0.103	0.097	0.092	0.103	0.086	0.096	0.045	0.041	0.047	0.152	0.004	0.003	0.003
K	0.008	0.002	0.001	0.000	0.001	0.012	0.001	0.002	0.001	0.001	0.000	0.000	0.000

MD, Monzodiorite; DO, Dolerite; IZ, Inclusion-rich zone; PX, Pyroxenite; XEN, Xenolith; BIZ, Between two inclusion-rich zones.

Table 3
U-Pb data

Mineral, characteristics[a]	Weight	U	Th/U[c]	Pbc	$^{206}Pb/^{204}Pb$[e]	$^{207}Pb/^{235}U$[f]	2σ	$^{206}Pb/^{238}U$[f]	2σ	rho	$^{207}Pb/^{206}Pb$[f]	2σ	$^{206}Pb/^{238}U$[f]	$^{207}Pb/^{235}U$[f]	$^{207}Pb/^{206}Pb$ [Ma][f]	2σ [abs]	Disc.
	[μg][b]	[ppm][b]		[pg][d]			[abs][f]		[abs][f]			[abs][f]					[%][g]
C-99-50 monzodiorite Lakseberga																	
Z eu lp fr [40]	27	467	1.3	19	11770	3.9770	0.0091	0.28481	0.00060	0.97	0.10127	0.00006	1615.6	1629.5	1647.6	1.0	2.2
Z an-sb eq-sp in [40]	13	596	0.8	4.6	29919	3.9680	0.0085	0.28434	0.00055	0.97	0.10121	0.00006	1613.2	1627.7	1646.4	1.0	2.3
Z an eq in [17]	9	536	0.6	10	8233	3.9465	0.0165	0.28333	0.00116	0.99	0.10102	0.00006	1608.1	1623.3	1643.0	1.2	2.4
Z eu lp fr [30]	42	497	1.2	41	8780	3.8137	0.0108	0.27451	0.00074	0.98	0.10076	0.00006	1563.7	1595.6	1638.2	1.0	5.1
M an eq p-y NA [1]	1	324	25	7.0	809	3.8104	0.0190	0.27396	0.00109	0.80	0.10087	0.00030	1560.9	1594.9	1640.3	5.6	5.4
M an sp p-y NA [3]	1	2549	101	3.8	11438	3.7684	0.0116	0.27181	0.00084	0.94	0.10055	0.00011	1550.0	1586.0	1634.3	2.0	5.8
M sb-an eq b NA [1]	1	941	98	1.8	7744	3.2393	0.0071	0.23820	0.00052	0.84	0.09863	0.00012	1377.3	1466.6	1598.4	2.3	15.4
M an eq br NA [5]	4	572	53	184	211	3.3776	0.0332	0.25011	0.00093	0.40	0.09794	0.00088	1439.1	1499.2	1585	17	10.3
C-99-55 foliated granite																	
Z sb-an sp [22]	25	336	0.5	4.4	34282	3.9879	0.0080	0.28546	0.00052	0.97	0.10132	0.00005	1618.8	1631.7	1648.4	1.0	2.0
Z eu sp [20]	29	309	0.6	8.8	18147	3.9513	0.0089	0.28312	0.00059	0.97	0.10122	0.00006	1607.1	1624.3	1646.6	1.1	2.7
Z eu(-sb) sp in [11]	37	182	0.6	7.2	16167	3.8529	0.0119	0.27673	0.00082	0.98	0.10098	0.00006	1574.9	1603.9	1642.2	1.0	4.6
M fr br NA [1]	10	518	27	2.4	38682	4.0006	0.0105	0.28797	0.00072	0.97	0.10076	0.00006	1631.4	1634.3	1638.1	1.1	0.5
C-99-51 pegmatite Lakseberga																	
Z fr flat [19]	150	222	0.0	13	10665	0.4833	0.0010	0.06404	0.00012	0.95	0.05473	0.00004	400.1	400.3	401.3	1.5	0.3
Z fr flat [16]	142	226	0.0	8.6	14953	0.4845	0.0014	0.06418	0.00016	0.92	0.05475	0.00006	401.0	401.1	401.9	2.5	0.2
M an p-y NA [1]	5	969	40	19	1022	0.4683	0.0026	0.06223	0.00024	0.73	0.05459	0.00021	389.2	390.0	395.3	8.6	1.6
M an p-y NA [1]	12	5198	6.4	14	75737	3.8244	0.0097	0.27705	0.00066	0.98	0.10012	0.00005	1576.5	1597.9	1626.2	0.9	3.4
C-99-53 metagabbro/dolerite dyke Andersvika																	
Z fr ang [2]	3	756	1.4	3.4	8424	2.2298	0.0051	0.19873	0.00045	0.88	0.08138	0.00009	1168.5	1190.5	1230.6	2.2	5.5
B fr flat NA [1]	1	195	0.07	4.9	330	1.294	0.012	0.12634	0.00053	0.54	0.07430	0.00059	767.0	843.2	1049.6	15.8	28.5
B fr eq [3]	8	55	0.06	4.2	720	1.0446	0.0073	0.10702	0.00055	0.63	0.07079	0.00039	655.4	726.2	951.3	11.2	32.7
Z rsb eq-sp [4]	2	163	0.4	1.2	1142	0.4941	0.0081	0.0636	0.0011	0.82	0.05631	0.00056	397.7	407.7	464.6	21.9	14.8
I an ang NA [> 50]	1798	0.50	1.6	631	22.19	0.48	0.26	0.0625	0.0037	0.11	0.056	0.031	391	399	——	——	13.0

[a] Z = zircon; M = monazite; B = baddeleyite; I = ilmenite; rsb = polycrystalline 'raspberry' aggregates; eu = euhedral; sb = subhedral; an = anhedral; eq = equant; sp = short pris,matic (l/w = 2-4); lp = long prismatic; fr = fragment; ang = angular; br = brown; p-y = pale-yellow; in = some inclusions; NA = not abraded, all others abraded; [N] = number of grains in fraction

[b] Weight and concentrations of grains below 2 ug are known to about +/- 50%

[c] Th/U model ratio inferred from 208/206 ratio and age of sample

[d] Pbc = total common Pb in sample (initial +blank)

[e] Raw data corrected for fractionation and blank

[f] Corrected for fractionation, spike, blank and initial common Pb (estimated from Stacey and Kramers (1975) model); error calculated by propagating the main sources of uncertainty

[g] Degree of discordance (in percent).

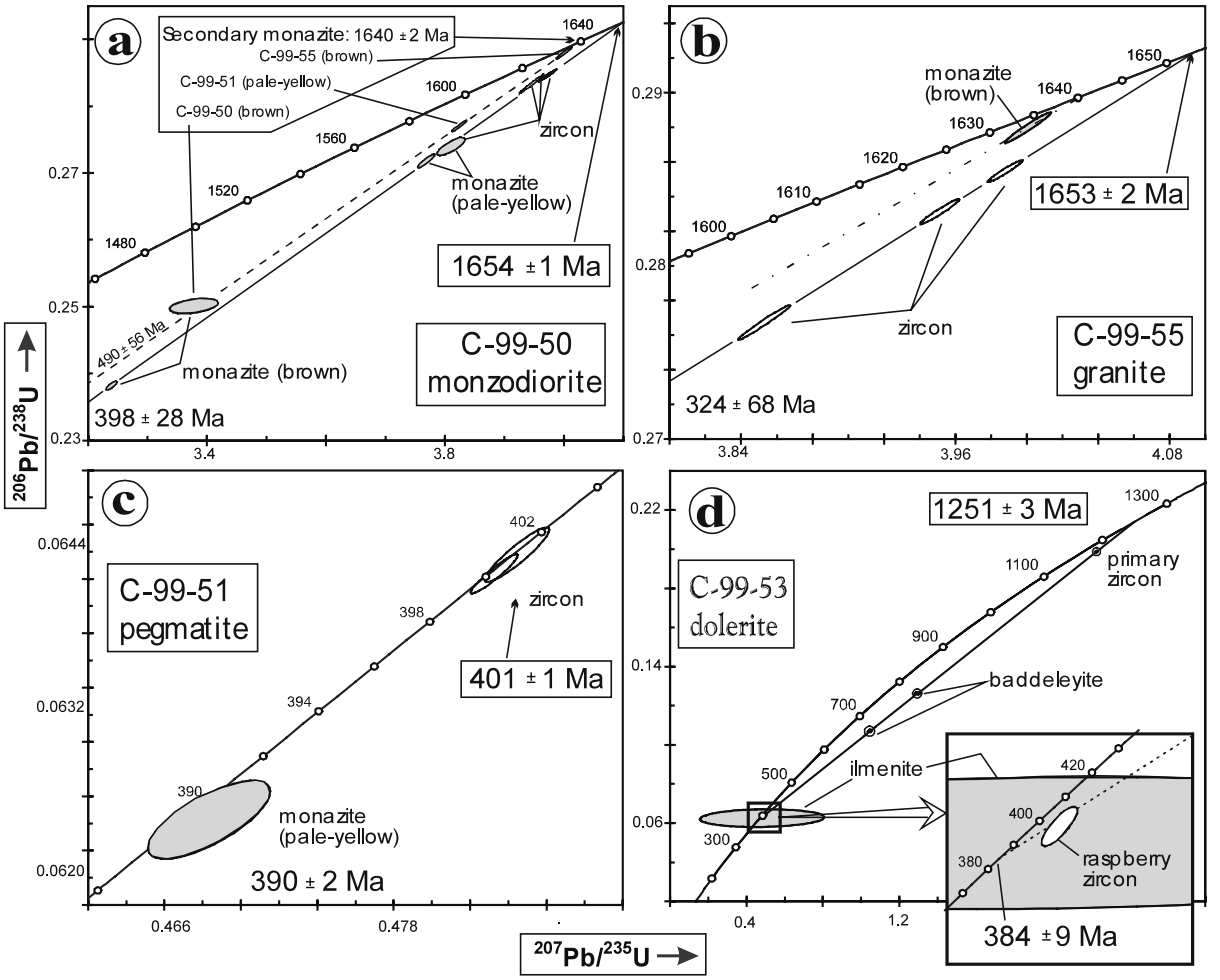

Fig. 4. Concordia diagrams with zircon, monazite, baddeleyite and ilmenite U–Pb data from Table 4. Ellipses indicate the 2σ uncertainty.

specific external appearance of the monazite. The main difference is that the data points of pale monazite are about 5.5% discordant, whereas those of brown monazite are 10–15% discordant. Three of the zircon and three of the monazite analyses are collinear defining an upper intercept age of 1654±1 Ma (Fig. 4a). The fourth zircon fraction, however, deviates to the left, increasing the MSWD from 0.7 to 3.3. A more distinct deviation is displayed by one of the analyses of monazite. The latter fraction, which consisted of five brown grains, displays a high common Pb content resulting in a poor precision, and fits on a discordia line defined by monazite analyses from the other two samples of the complex. The possible interpretation is, therefore, discussed below.

6.2. Granite (C-99-55)

The granite contains a relatively uniform population of equant to short prismatic zircon with euhedral to somewhat subrounded crystal shapes. The amount of inclusions is moderate and there are local hints of potential cores. The three zircon fractions analysed contain about 200–300 ppm U, display intermediate Th/U ratios, and are between 2 and 5% discordant, defining a discordia line with an upper intercept of 1653±2 Ma (Fig. 4b). In

contrast to the monzodiorite, there is almost no monazite in this sample. Most of the potential monazite grains are highly altered and only one grain appeared to be suitable for analysis. This is a brown fragment, of similar appearance as the brown monazite in the monzodiorite. The analysis is nearly concordant with a $^{207}Pb/^{206}Pb$ age of 1638 ± 1 Ma, younger than coexisting zircon, and fits a line drawn through monazite from the pegmatite dyke (see below) and the one deviant analysis from the monzodiorite (Fig. 4b).

6.3. Pegmatite (C-99-51)

The zircon population in the pegmatite comprises mainly high quality, clear and crack-free zircon ranging from perfectly euhedral, short prismatic gems to more complex, multifaceted to irregular anhedral grains. Potential cores were observed locally. Two analyses were carried out on relatively flat zircon fragments chosen in an attempt to circumvent possible inheritance, yielding two concordant analyses at 401 ± 1 Ma (Concordia age of 400.6 ± 0.6 Ma, Ludwig, 1999; Fig. 4c). As in the granite, there are just very few grains of clearly identifiable monazite in this sample and only two grains could be analysed. One of the analyses yields a Precambrian age, plotting on the subsidiary monazite line together with one analysis each from monzodiorite and granite. By contrast, the second monazite analysis is concordant at 390 ± 2 Ma, clearly postdating the zircon age (Fig. 4c).

6.4. Dolerite (C-99-53)

The dolerite contains small amounts of baddeleyite, which shows all degrees of transformation to polycrystalline (raspberry) zircon as previously described by Davidson and van Breemen (1988) and Heaman and LeCheminant (1993). The polycrystalline zircon (baddeleyite pseudomorph) has a yellowish, translucent appearance, and in part it contains cores of unreacted baddeleyite. These features distinguish it from a second type of zircon consisting of limpid crystals and fragments, locally exhibiting cracks and altered domains. A fraction of two similar abraded transparent zircon fragments yields a 5.5% discordant analysis, whereas two fractions of baddeleyite, a single unabraded grain and a fraction of three abraded grains, are much more discordant but perfectly collinear with the zircon analysis (Table 3 and Fig. 4d). One analysis was done on a two-grain fraction of baddeleyite-free raspberry zircon yielding a data point near the lower end of the line.

Zircons also occur as 10–20 μm sized inclusion in ilmenite. In ilmenite grains that preserve their magmatic shape the inclusions of zircons are found as fracture trails typically together with small inclusions of biotite and carbonates. During recrystallisation of the ilmenite the linear arrangement along fractures are broken and they appear more randomly inside the ilmenite grains. Ilmenite grains with zircon inclusions were analysed and gave a similar position as the raspberry zircons, but with much less precision (Table 3 and Fig. 4d) due mainly to the low U content of 0.50 and 0.33 ppm initial Pb. Monazite grains up to 30 μm occur associated with apatite.

The upper intercept of 1251 ± 3 Ma (1252 ± 4 Ma using only the uppermost zircon and baddeleyite analyses) dates the magmatic emplacement of the dolerite (Fig. 4d). The significance of the lower intercept age is somewhat more uncertain: in fact the regression through primary zircon and baddeleyite analyses yields a lower intercept age of 391 ± 12 Ma, which overlaps within error the age of the pegmatite. Inclusion of the raspberry zircon analyses modifies the intercept to 384 ± 9 Ma, but because the raspberry zircons could not be abraded (without disintegrating), this lower intercept could be biased downward by some secondary Pb loss and is thus less reliable. Inclusion of the ilmenite result in the regression does not affect the age values. The ilmenite age itself (Concordia age of 391 ± 22 Ma) is too imprecise to help in the resolution of the Caledonian event.

7. Rb–Sr data

7.1. Analytical procedure

The rocks were crushed in a steel-jaw crusher and finely ground in a tungsten carbide mill. For

Table 4
Whole-rock Rb–Sr and Sm–Nd data

Sample	Rock type	Rb (ppm)	Sr (ppm)	$^{87}Rb/^{86}Sr$	$^{87}Sr/^{86}Sr$	Sm (ppm)	Nd (ppm)	$^{147}Sm/^{144}Nd$	$^{143}Nd/^{144}Nd$	ε_{Nd} (T)	for T (Ma)
FAR-2	QM	47	1045	0.130	0.705672	2.22	14.02	0.09602	0.511665	2.4	1654
FAR-3	GR	129	366	1.02	0.725753	3.12	20.84	0.09091	0.511581	1.8	1654
FAR-4	GR	88	537	0.470	0.713443	7.20	37.42	0.11673	0.511907	2.7	1654
FAR-5	GR	167	340	1.43	0.735889	3.54	22.65	0.09490	0.511637	2.1	1654
FAR-6	GR	161	332	1.41	0.736042						
FAR-7	GR	170	330	1.49	0.737830						
FAR-8	GR	159	321	1.44	0.736390						
FAR-9	GR	166	323	1.49	0.737210						
FAR-10	GR	158	339	1.35	0.733446						
FAR-12	GR	155	346	1.30	0.732828						
FAR-13	GR	145	339	1.24	0.731178						
FAR-14	MD	69	886	0.230	0.707908						
FAR-15	MD	65	975	0.190	0.707099						
FAR-16	MD	62	983	0.180	0.706857						
FAR-17	QM	57	1088	0.150	0.706180						
FAR-18	MD	97	765	0.370	0.710998						
FAR-19	MD	80	790	0.290	0.709542						
FAR-20	GR	184	313	1.71	0.742819						
FAR-21	QM	57	832	0.200	0.707085						
FAR-22	DO	11	412	0.070	0.704463	4.61	18.67	0.15040	0.512333	1.5	1251
FAR-24	QM	69*	1137*	0.174	0.706649	7.24	40.43	0.10896	0.511759	1.5	1654
FAR-26	GR	165	325	1.47	0.735637						
FAR-31	MD	106	776	0.390	0.712119	7.23	39.65	0.11090	0.511823	2.3	1654
FAR-33	MD	100	773	0.400	0.711853	7.42	40.43	0.11170	0.511823	2.1	1654
FAR-35C	GR	153	519	0.850	0.722168						
FAR-37B	DO	24*	316*	0.220	0.707270	7.83	32.11	0.14850	0.512260	0.4	1251
FAR-38A	XEN	11*	689*	0.044	0.703886	1.42	7.41	0.11674	0.511809	0.8	1654
FAR-38B	XEN	4.5*	1187*	0.011	0.702936	1.11	5.15	0.13153	0.511930	0.0	1654
FAR-38D	XEN	4.1	540	0.022	0.703631	2.07	7.41	0.16986	0.512367	0.4	1654
FAR-39A	PEG	29	932	0.089	0.710952						
FAR-39B	PEG	175	1179	0.430	0.713144						
FAR-39C2	PEG	67	1096	0.180	0.711525						
FAR-39C1	PEG	107*	1363*	0.240	0.711972	0.18	1.02	0.10982	0.511762	−12.7	401
FAR-39D	PEG	158	1022	0.450	0.713270						
FAR-39E	PEG	101	1023	0.290	0.712323						
FAR-46A	PX	14*	159*	0.260	0.709186	1.96	8.83	0.13504	0.512038	1.4	1654
FAR-46B	PX	15*	157*	0.270	0.709396	1.97	8.89	0.13504	0.512041	1.4	1654

DO, dolerite; GR, granite; MD, monzodiorite; QM, quartz-monzonite; PEG, pegmatite; PX, pyroxenite; XEN, xenolith: Rb and Sr concentrations measured by XRF except those marked by asterisk (*), which were analysed with isotope dilution; eNd(T): deviation of measured from chondritic value at time T (in parts per 10 000).

samples with more than 30 ppm Rb the Rb/Sr ratio was generally determined by precise X-ray fluorescence method, using Compton top matrix correction, and $^{87}Sr/^{86}Sr$ was obtained from unspiked measurements. The Rb and Sr contents of samples with Rb < 30 ppm were determined by isotope dilution using a mixed $^{87}Rb/^{84}Sr$ spike. Variable mass discrimination in $^{87}Sr/^{86}Sr$ was corrected by normalising $^{88}Sr/^{86}Sr$ to 8.3752. The samples were analysed with a VG 354 multicollector mass spectrometer. The ^{87}Rb decay constant used is 1.42×10^{-11} per year, and the data have been regressed with the program of Ludwig (1999). In assigning errors to the data points the coefficient of variation is taken as 1% for the $^{87}Rb/^{86}Sr$ and 0.005% for $^{87}Sr/^{86}Sr$ (2σ). Age and intercept errors are quoted at the 2σ confidence level.

8. Results

Rb–Sr data from the various rock types of the HIC, including three xenoliths, two samples of dolerite and six pegmatites, are listed in Table 4 and plotted in isochron diagrams in Fig. 5. Regression of the data for granitic samples alone defines a line corresponding to an age of 1656 ± 49 Ma with an I.R. of 0.70193 and a MSWD value of 6.6 (omitting sample FAR 26) (Fig. 5a). This age is identical to the U–Pb zircon age but with a higher uncertainty. Regression of the data for all the other samples, but without the granite, yields an age that is similar within error, but has a much greater scatter (MSWD = 83; Fig. 5b). Combining all the analyses in one regression changes the age to 1610 ± 18 Ma with an I.R of 0.70275 and a MSWD value of 50. As is apparent from Fig. 5b the pegmatites define a less steep line corresponding to an age of 452 ± 26 Ma with a relative high I.R of 0.7104 and MSWD of 4.3. This age is significantly older than the U–Pb zircon age of 401 ± 1 Ma and inferred to be the age of the pegmatites, thus it likely implies a heterogeneous initial Sr composition. The high I.R. and negative ε_{Nd} of −12.7 (see below) also shows that the pegmatite swarm formed from material with a long crustal history. The trend of constant or increasing Rb/Sr ratios with increasing Sr (Table 4) is different from that of a normal fractionation trend and the fact that all pegmatite data plot to the left of the array defined by the HIC samples tends to suggest that the melts cannot have been derived as partial melts from the HIC. It is, however, possible that the melts may have been produced under water saturated conditions, keeping mica (hence Rb) in the residue and producing low Rb/Sr melts (Prince et al., 2001).

9. Sm–Nd whole rock data

9.1. Analytical procedure

The analytical procedure for the Sm–Nd work follows that described by Mearns (1986). Isotope ratios have been measured using a VG354 multicollector instrument and normalised to $^{146}Nd/^{144}Nd = 0.7219$, using a decay constant for ^{147}Sm of 6.54×10^{-12} per year. Data regressions were done with the program of Ludwig (1999) using error estimates of 0.05% for $^{147}Sm/^{144}Nd$ and 0.005% for $^{143}Nd/^{144}Nd$ (2σ). ε_{Nd} values were calculated relative to CHUR with present-day $^{147}Sm/^{144}Nd = 0.1967$ and $^{143}Nd/^{144}Nd = 0.512647$.

10. Results

Sm–Nd data for a limited number of samples are shown in Table 4, together with calculated model ages, and $\varepsilon_{Nd,1654}$ and are plotted in an isochron diagram in Figs. 6 and 7. Regression of the seven samples belonging to the evolved parts of the HIC defines a line which corresponds to an age of 1754 ± 330 Ma (MSWD 2.8). The high uncertainty in the age is related to the limited spread in $^{147}Sm/^{144}Nd$. By including the three xenolith and two pyroxenite samples an age of 1464 ± 160 Ma is calculated but the MSWD increases to seven. A line based on the evolved members and the two samples of pyroxenite corresponds to an age of 1555 ± 180 Ma (MSWD = 3.3). As for the Rb–Sr data, the results for the most felsic members of the complex yield ages that are closest to the magmatic

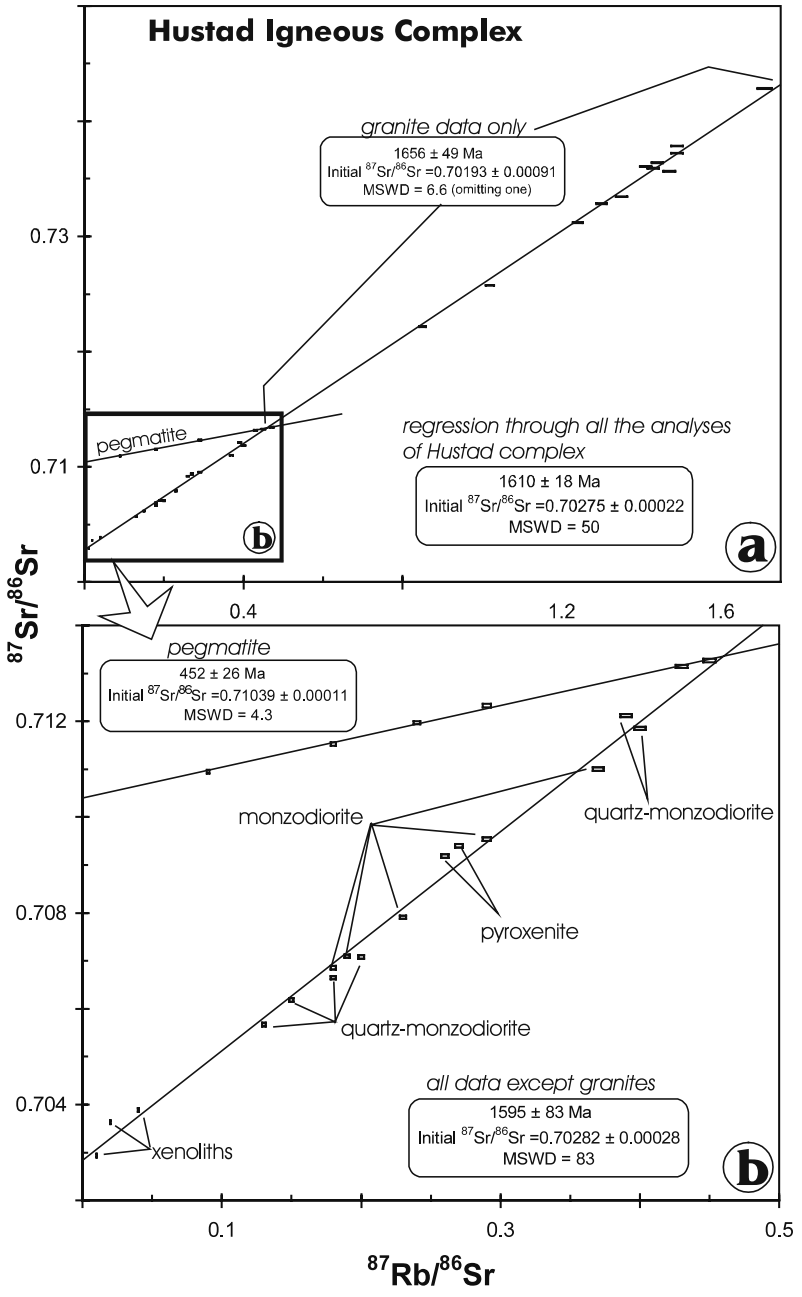

Fig. 5. (a, b). Rb–Sr isochron plots for the HIC.

age as defined by zircon, whereas the data for the mafic units tend to tilt the lines towards younger ages, indicating either the effects of metamorphic disturbances or initial isotopic heterogeneity. These relationships will be discussed more extensively below.

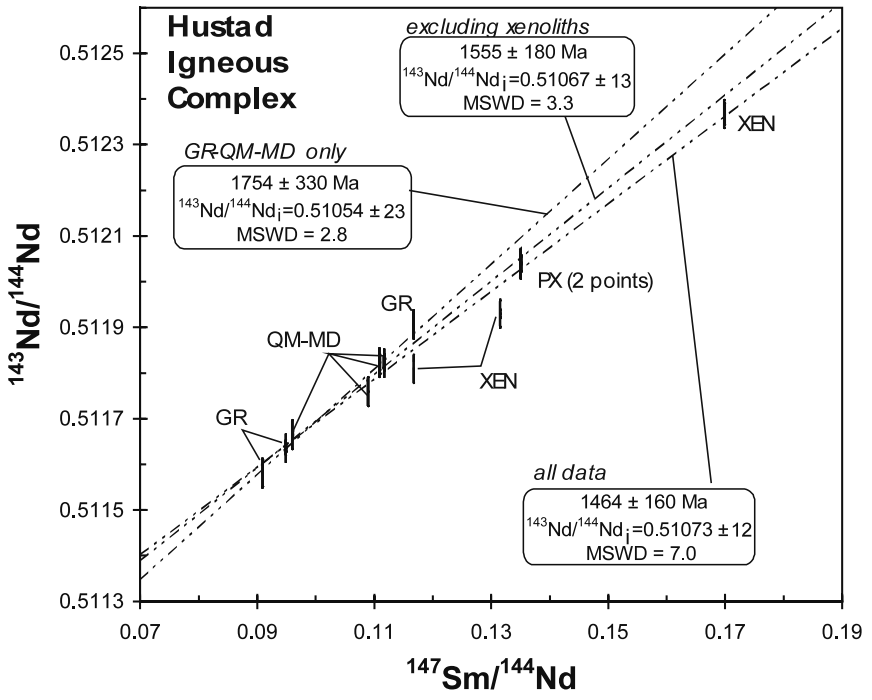

Fig. 6. Sm–Nd isochron diagram for the HIC (GR, granite, MD, monzodiorite, QM, quartz-monzonite, PX, pyroxenite, XEN, xenolith).

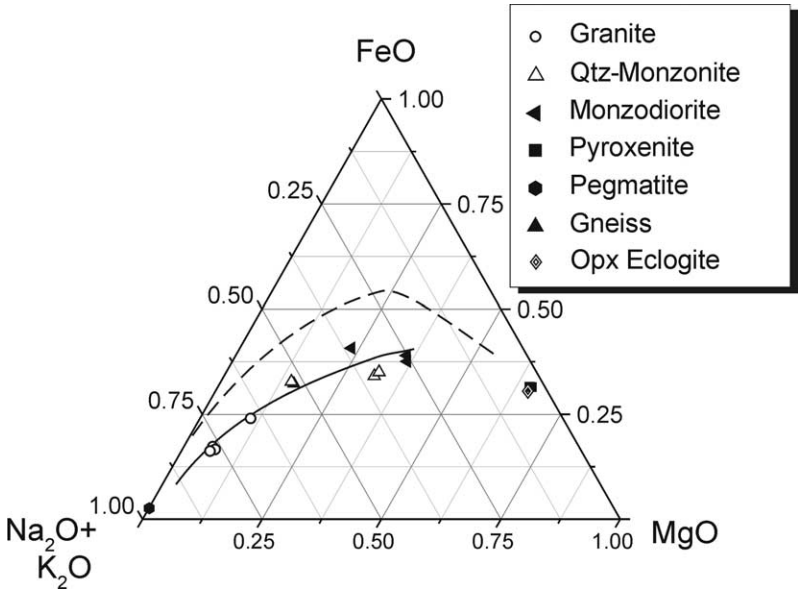

Fig. 7. AFM diagram for the Hustad complex. Also shown are the Dråga gneiss and the average of three orthopyroxene eclogites from the Moldefjord area given by Carswell and Harvey (1985). The data are compared with the calc alkaline series (full line) and the tholeiitic series (stippled line), represented by the Lorne and the Thingmuli lavas, respectively. The latter data are from Groome and Hall (1974), Carmichael (1964).

11. Interpretation of isotope ages

The zircons in the granite and the monzodiorite, together with three monazite analyses in the latter sample, yield overlapping ages of 1654±1 and 1653±2 Ma (Fig. 4a and c), which are interpreted to date the time of magmatic emplacement of the HIC. The Rb–Sr and Sm–Nd whole rock dates are in accordance with this, although these ages are less precise (Figs. 5 and 6).

The upper intercept age of 1640±2 Ma defined by monazite analyses in each of the three samples requires a more speculative interpretation. The brown monazite analysed in the granite is essentially the only suitable grain that could be recovered from that sample, and it is, therefore, legitimate to ask whether this could just be a contaminant derived from the monzodiorite where such grains are common. In fact, one analysis from the latter sample that fits this subsidiary monazite line consisted of a similar type of grains, albeit with a much higher amount of common Pb and much more discordant. The other single brown monazite from the monzodiorite is also very discordant, but fits on the primary discordia line. Thus the contamination hypothesis is not well supported by the data. The alternative is that the deviant monazites reflect secondary growth or resetting at 1640 Ma, perhaps in local micro-veins as a response to post-magmatic fluid activity. At the moment this represents our preferred interpretation.

The two analyses of monazite from the pegmatite dyke lend themselves to similar kinds of speculations. The pale-yellow monazite yielding the Precambrian age and fitting the subsidiary 1640 Ma line is clearly of inherited origin because the zircon data demonstrate that the dyke is a Caledonian intrusive rock (Fig. 4a and c). Lab contamination seems to be unlikely, as the corresponding clear monazite grains present in the monzodiorite are much smaller than those from the dyke and yield primary (1654 Ma) ages rather then reflecting the secondary event. An explanation that seems to fit better this unlike bits of information is that the monazite found in the dyke grew originally in micro-fractures developed during cooling of the complex from late- or post-magmatic solutions. These micro-fracture systems were then reactivated during Caledonian deformation and exploited as conduits by the ascending melts, which scavenged the exposed vein monazite before their crystallisation as granitic pegmatites. The 452±26 Ma Rb–Sr whole rock age obtained from the pegmatites may support mixing and a lack of complete homogenisation of the Sr isotopes.

The Precambrian zircons and monazites are all variously discordant and this can be logically attributed to the effects of the Caledonian events. Especially the monazites, which were not abraded, will easily reflect any effect in near-surface domains. The discordance may reflect either diffusion of Pb, or local recrystallisation with expulsion of Pb, or growth of thin metamorphic rims (e.g. Crowley and Ghent, 1999). By contrast, it is more difficult to explain the 390 Ma monazite in terms of Pb loss after 401 Ma, as the region has not, according to Tucker et al. (1986/1987), been affected by a high-grade event since then. However, we are aware that fluid circulation may be equally effective as temperature in reequilibrating isotopic systems. It is likely that the monazite in the pegmatite dates the secondary alteration outlined above as manifested by formation of calcite, sericite and euclase. The growth of raspberry zircon from baddeleyite and formation of zircons together with carbonates and biotites in ilmentite of the dolerite also demonstrate the role of fluids and deformation on the minerals (zircons and baddeleyite) used for U–Pb dating. Taken at face value the lower intercept age of 384±9 Ma defined by baddeleyite and two zircon types in the dolerite (Fig. 4d), suggest that the rock underwent its main metamorphic recrystallisation event during the same late-Caledonian period. However, as pointed out above, it is possible that the lack of abrasion of the raspberry zircons may have biased the lower intercept towards a too low intercept. The growth of secondary zircons in and on ilmentite grains has recently been demonstrated from the Bergen Arc (Fig. 1), another high-grade metamophic area (Bingen et al., 2001). The reason for zircon to grow on and in ilmenite is not obvious. Zirconium may have been exolved from ilmentite and formed zircons through interaction with the fluid or

zircons may simply have been deposited by the fluid in a chemically 'attractive' environment.

Although only two Sr and Nd isotope analyses were done on samples from the dolerite, the results show some interesting contrasts. A line calculated through the two Rb–Sr analyses (not shown) corresponds to an age of about 1300 Ma, which is close to the actual age (1251 Ma) of the sample, whereas a regression through the two Sm–Nd analyses yields a very steep and unrealistic slope. Calculated ε_{Nd} values (at 1251 Ma) range from +0.4 to +1.5 (Table 4) indicating either that the source was isotopically highly evolved (e.g. sub-continental mantle), or that the magma underwent widespread contamination during emplacement in the crust, or that the metamorphic overprint seriously disturbed the Sm–Nd system in these rocks.

12. Whole rock geochemistry

12.1. Major elements

Whole-rock major, minor and trace element data for the various rock types of the HIC together with one sample of nearby Dråga gneiss and the average opx-eclogites from the Molde area as calculated by Carswell and Harvey (1985) are presented in Table 5. The data reveal a wide range of major elements with SiO_2 varying from approximately 52–72 wt.%. The complex is characterised by a high MgO content at fixed SiO_2 value (monzodiorite with 54 wt.% SiO_2 contains 7.5 wt.% MgO), and high *mg*-numbers ranging from approximately 0.40 for the granite through 0.62 for the monzodiorite and quartz-monzonite, reaching 0.80 in the pyroxenite. According to the geochemical classification of Frost et al. (2001) for granitic rocks the HIC classifies as magnesian. They are all metaluminous (ASI < 1) except for the pegmatite that is slightly peraluminous. The K_2O+Na_2O contents are high and the evolved members have $K_2O/Na_2O > 1$. The HIC exhibits a trend on an AFM diagram (Fig. 7) very similar to that of the calc-alkaline trend as represented by Californian batholiths (Larsen, 1948), or by the Lorne lavas (Thirlwall, 1982). As pointed out by Frost et al. (2001) this is in accordance with their magnesian nature. Peacock (1931) index straddles the border between calc-alkaline and alkali-calcic rocks and with the modified alkali-lime index (MALI) of Frost et al. (2001) the HIC rocks plot in the fields of alkali-calcic and calc-alkalic. In the classification of Brown (1982) the complex follows the AFM trend for plutonic rocks of high arc maturity and it plots within the field of high-K calc-alkaline magmas defined by Peccerillo and Taylor (1976) (9). This is much higher than the Tuolumne plutonic complex of the Sierra Nevada (Bateman and Chappell, 1979) and similar to the high-K Caledonian granite complexes of the British Isles (Halliday and Stephens, 1984). However, the complex is lower in K than shoshonite found in island arcs (Smith, 1972). Most samples are quartz-normative except for sample Far-15, which is olivine normative.

12.2. Trace elements

Trace elements including REE concentrations for seven samples of the HIC and one sample of Dråga gneiss are presented in Table 5. The REE were determined by NAA following the radiochemical separation method described by Brunfelt et al. (1974), Krogh and Brunfelt (1981). In a chondrite normalised diagram (Fig. 10) the monzodiorite displays a smooth concave or U-shaped REE pattern, typical for calc-alkaline magmas from which amphibole has fractionated (Schnetzler and Philpotts, 1970). A similar REE pattern has been reported by Skår (2000) from the southern part of the WGR. A light to heavy REE fractionation, suggested by Ce_N/Yb_N ratios of 10, is present in the granite, quartz-monzonite and monzodiorite. A slight positive Eu anomaly is found in granite and quartz-monzodiorite, while the pyroxenite displays a negative Eu anomaly (Fig. 9). The Dråga gneiss has the same REE characteristics as the felsic members of the Hustad complex. The total REE contents (Table 5) decrease from monzodiorite, through quartz-monzonite to granite, the reverse of normal igneous trends, indicating that the REE behaved as compatible elements. Stephens et al. (1985) describe similar relationships for the zoned Criffell

Table 5
Major and trace element composition of the Hustad complex

Sample	FAR3	FAR5	FAR20	FAR35C	FAR23	FAR31	FAR33	FAR15	FAR19	FAR46A	FAR46B	FAR21	FAR22	FAR39D	DRÅ1	B
Rock type	GR	GR	GR	GR	QM	QM	QM	MD	MD	PX	PX	MD	DO	PEG	Gneiss	MG
SiO_2	71.11	71.16	71.74	66.33	57.62	56.7	56.57	51.79	53.95	51.96	51.85	53.57	45.31	72.3	60.64	50.06±1.33
TiO_2	0.22	0.23	0.22	0.41	0.79	0.7	0.72	0.85	0.77	0.33	0.33	0.8	1.96	0.02	0.72	0.29±0.04
Al_2O_3	14.2	14.51	14.35	15.49	18.24	14.4	14.39	14.4	13.85	7.55	7.45	18.55	15.94	14.42	17.13	8.50±0.78
Fe_2O_3	0.43	0.59	0.44	1.49	2.09	2.36	2.67	2.5	2.68	2.73	2.55	2.37	4.79		1.61	1.75±0.26
FeO	1.31	1.27	1.49	1.75	3.17	4.5	4.38	6.24	5.51	7.1	7.28	5.04	9.15	0.32	3.56	7.62±1.14
MnO	0.06	0.06	0.07	0.07	0.09	0.12	0.12	0.16	0.15	0.2	0.21	0.15	0.2	0.01	0.1	0.19±0.01
MgO	0.6	0.71	0.63	1.35	2.23	5.92	6.04	7.45	7.44	18.89	19.02	3.97	7.45	0.01	2.32	18.52±1.02
CaO	1.99	1.91	1.84	2.64	5.13	5.97	5.99	7.93	7.1	6.9	7	6.18	9.29	0.25	4.56	10.12±0.18
Na_2O	2.8	3.3	3.3	3.8	3.9	3.1	2.9	2.9	2.9	0.5	0.4	4.1	2.7	1.6	3.8	0.76±0.11
K_2O	4.87	4.66	4.64	4.53	4.02	3.38	3.31	2.34	2.34	0.42	0.4	1.99	0.75	9	3.99	0.42±0.25
P_2O_5	0.05	0.06	0.05	0.11	0.39	0.28	0.28	0.38	0.31	0.04	0.03	0.33	0.28	0.01	0.31	0.34±0.37
LOI	0.5	0.47	0.3	0.45	0.71	0.85	0.78	1.37	1.17	1.81	1.12	1.68	1.48	0.17	0.7	0.89±0.60
Total	98.14	98.93	99.07	98.42	98.38	98.28	98.15	98.31	98.17	98.43	97.64	98.73	99.3	98.11	99.44	99.46
Mg-no	40	42	39	44	45	62	62	62	63	79	79	51	51	6	46	79
Cs*	2.9	4.1				18.8			23.2		33.2	19.3			12.7	
Rb	129	167	184	153	92	106	100	65	80	14	15	57	11	158	111	23±4
Sr	366	340	313	519	1100	776	773	975	790	159	157	832	412	1022	770	
Ba	915	900	824	938	1800	1200	1000	1500	1100	138	147	492	500	5000	1200	149±83
Zr	122	133	126	232	161	195	194	149	169	46	50	181	127	25	221	30±8
Hf*	3	3.6				3.5			3.9		1.2	4.6			5.3	
Th*	7	10.4				5.4			3.5		1.5	2.9			7	
U*	0.5	2.1				1.8			1.3		0.3	1			1.6	
La*	26.6	30.1				72.7			38		7.4	34.9			47.4	
Ce*	56.3	67.1				88.4			77.6		20.2	67.5			110.1	
Nd**	20.8	37.4				39.7					8.8	18.7				
Sm*	3.1	3.9				6.7			6.7		1.9	5.4			7	
Eu*	1.4	1.4				2.2			2		0.3	2.1			2.5	
Tb*	0.35	0.45				0.9			0.65		0.25	0.55			0.9	
Yb*	2	3.3				5.9			4		2.2	3.5			4	
Lu*	0.23	0.49				0.89			0.5		0.28	0.37			0.43	
Cr	140	162	98	115	104	402	398	446	508	1600	1600	123	158	140	112	1960±55
Ni	7	7	6	11	31	129	27	143	147	778	800	40	145	6	28	498±41
Co*	3.2	3.9				28.3			33.1		71.7	23.3			14.9	
Cu	< 5	< 5	< 5	22	129	84	112	150	168	118	144	10	56	< 5	81	29±11
Sc*	2.9	4.1				18.8			23.2		33.2	19.3			12.7	
V	28	29	26	55	148	180	173	231	200	133	134	169	223	17	128	315±139
Zn	30	34	29	47	62	70	71	96	85	82	82	102	116	< 5	66	86±13
Y	11	17	14	24	21	22	24	24	24	13	14	22	29	< 5	27	8±6
Nb	10	11	13	15	14	13	15	11	10	6	7	8	5	< 5	16	
Ta*	0.5	0.7				0.7			0.5		0.2	0.4			0.9	

Abbreations same as Table 4. B: Average with 1s of three eucritic opx eclogites, from Carswell and Harvey (1985). *, NAA. **, I.D.

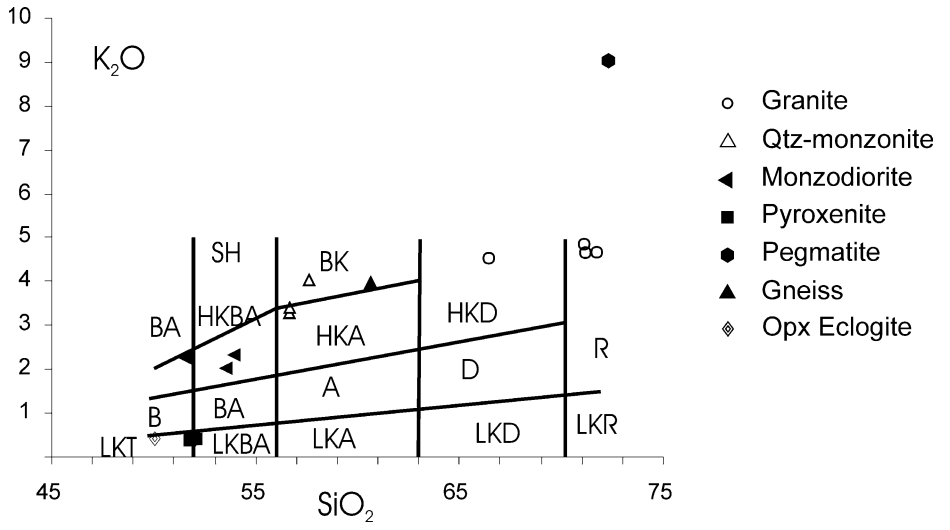

Fig. 8. K_2O vs. SiO_2 diagram illustrating the potassium-rich nature of the HIC and the Dråga Gneiss with fields of Peccerillo and Taylor (1976).

pluton of the British Isles and interpreted this as increasing contamination by anatectic crustal magmas. For the HIC a similar explanation would require contamination by juvenile crust in order to comply with the observed low Sr initial ratios.

In the multi-element variation diagram (Fig. 10) the rocks of the HIC and the Dråga gneiss display the characteristic negative Nb–Ta anomaly typical for igneous rock formed at destructive plate margins but they differ from the latter by showing positive anomalies for Ba and Sr (Fig. 10). It is to be noted that the Ba and Sr characteristics also apply to the Dråga gneiss and particularly to the pegmatite where Ba reaches 5000 ppm (Table 5). The rocks display normal to high K/Rb ratios ranging between 209 and 365. The analysed xenoliths have low Rb (4–11 ppm) and high Sr (550–1300 ppm) contents. Their Sm and Nd contents (Table 4) are comparable to those of the pyroxenites and reflect the high content of mafic

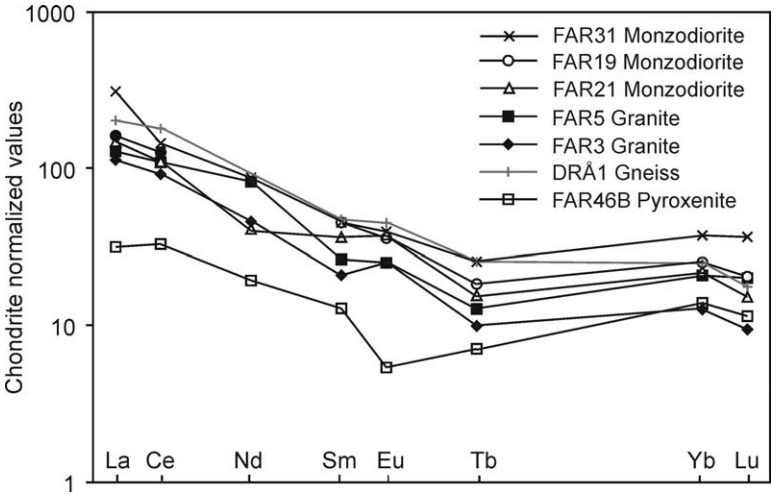

Fig. 9. Chondrite normalised REE-pattern of various rocks of the HIC.

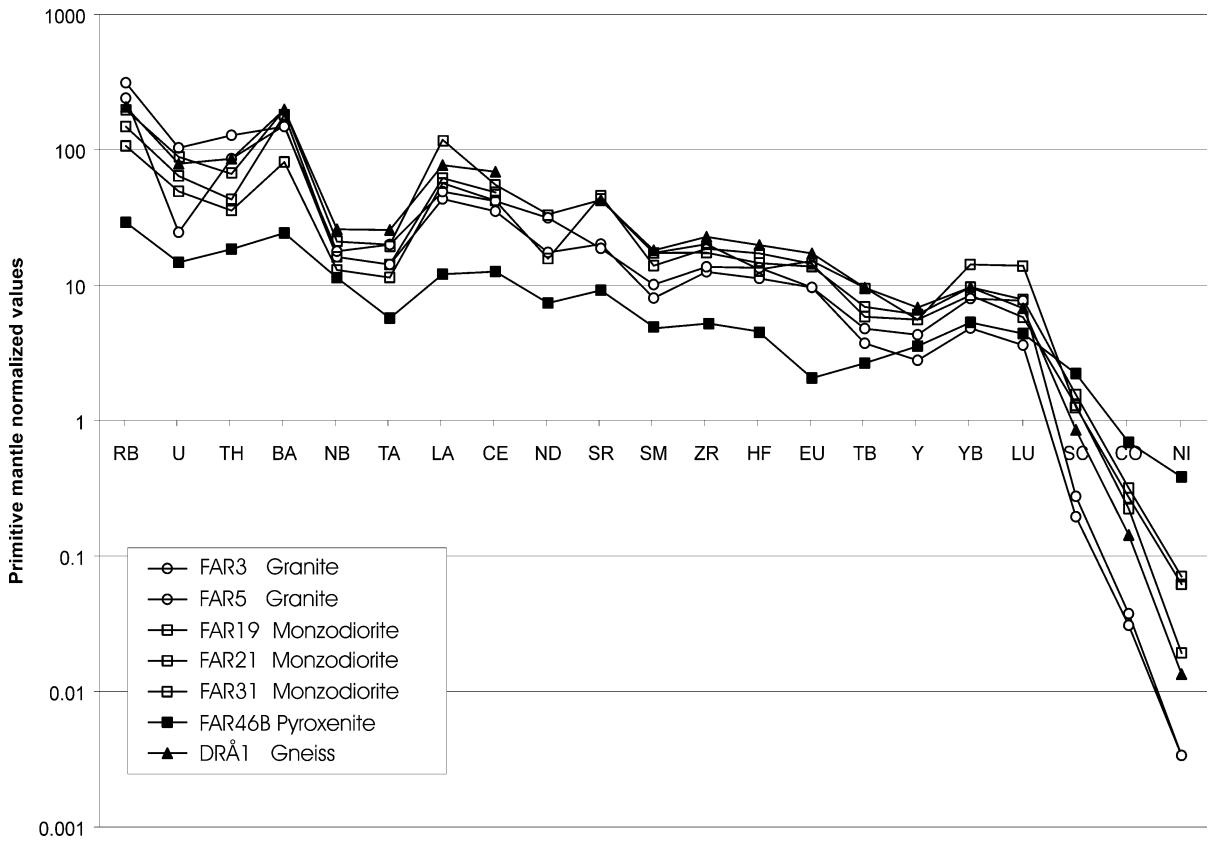

Fig. 10. Multi-element variation diagram illustrating the geochemical characteristics of the various rocks types of the HIC and the Dråga gneiss. Normalising values after Hofmann (1988).

phases including garnet, pyroxene and amphibole. The heat producing elements Th and U are present in low to moderate amounts with Th increasing from 1.5 ppm in the pyroxenite to 10 ppm in the granitic rocks and Th/U ratios varying between 2.9 and 13 (Table 5) compared with a bulk crust ratio of 3.8 (Taylor and McLennan, 1985).

The HIC contains high Cr and Ni values at a fixed SiO_2 content (Table 5). In the analysed pyroxenites Cr and Ni values are 1600 and 800 ppm, respectively. This is in accordance with the presence of pentlandite grains and elevated Cr values (up to 1 wt.%) in both ortho- and clinopyroxene (Table 2). The high Ni and Cr contents extend to the more felsic members of the complex where the monzodiorite sample FAR 19, with 54% SiO_2, contains 508 ppm Cr and 147 ppm Ni and the granites in average have more than 100 ppm Cr.

13. Isotope systematics

The initial $^{87}Sr/^{86}Sr$ ratio of 0.7019 ± 0.0009 defined by the felsic rocks of the HIC overlap the depleted mantle composition at this time whereas the corresponding ε_{Nd} values are some 2 ε-units lower than that (Fig. 11a). Overall this relationships are consistent with a derivation of the granitic to quartz-monzonitic core of the complex either from a slighly evolved mantle source or from juvenile (late Svecofennian) crust without significant contribution of much older continental crust (Fig. 11b). The lack of inherited

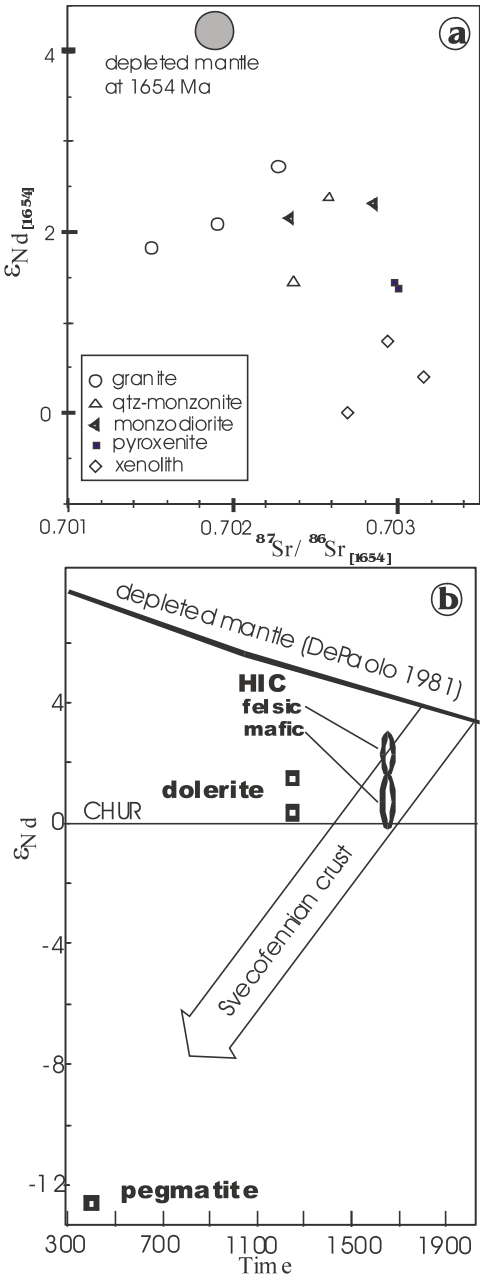

Fig. 11. (a) Diagram for the initial Nd and Sr characteristics of the HIC. The depleted mantle values are calculated from present day values of $^{87}Rb/^{86}Sr = 0.03$ and $^{87}Sr/^{86}Sr = 0.7026$. (b) Isotopic evolution of Nd vs. time diagram with data for the HIC, the pegmatite and the two dolerite samples. The trajectory describing Svecofennian crustal development is taken from Andersen and Sundvoll (1995).

cores in the zircon populations support this interpretation. The interesting aspect of the data is the fact that the felsic components of the HIC yield lower $^{87}Sr/^{86}Sr$ and higher ε_{Nd} than the pyroxenites and xenoliths, without any notable difference between the clear cumulates and the banded xenoliths (Fig. 11a). There is thus no positive correlation between a normal liquid line of descent and ε_{Nd} values, as would be expected if the granites contained an increasing component of contaminating older crust compared with the pyroxenites, unless one assumes that the mafic rocks were derived from an isotopically more evolved mantle domain (e.g. older enriched sub-continental mantle lithosphere) and were contaminated with juvenile felsic crust (recent magmatic arc material).

One explanation could be that the xenoliths, which have the lowest ε_{Nd} (around zero) and the highest $^{87}Sr/^{86}Sr$ initial ratios of 0.703, are older than the HIC. An older age would result in a more positive e_{Nd} value, but since the xenoliths have lower Rb/Sr ratios (0.01–0.04) than the mantle their higher initial $^{87}Sr/^{86}Sr$ will increase rather then decrease, which is paradoxal.

An alternative explanation may be that the Rb–Sr and Sm–Nd ratios of the mafic rocks in the HIC were modified during Caledonian metamorphism. Orthopyroxene eclogites from the WGR, to which the pyroxenites bear a strong geochemical resemblance, display elevated initial $^{87}Sr/^{86}Sr$ (Brueckner, 1977). Several of the orthopyroxene eclogites studied by Griffin and Brueckner (1985) display high Sr I.R. of around 0.715 that according to the authors could be explained either by Rb loss or by gain of radiogenic Sr. The pyroxenites of the HIC only display minor reactions and plot only slightly above the regression line. They have markedly higher Rb than the orthopyroxene eclogites with high I.R. suggesting that the latter have lost Rb during the eclogite facies event. Conversely, it may also mean that the higher I.R. and lower ε_{Nd} of the pyroxenites compared with the granites of the HIC is related to Rb loss during the Caledonian metamorphism rather than being a primary feature. One process that could contribute to lower Rb/Sr and increase Sm/Nd ratios is the formation of garnet, for

example by reactions that consume plagioclase liberating elements that are incompatible in the garnet structure such as LREE and Rb (e.g. Mørk and Mearns, 1986). These elements could then be lost from the rock when fluids leave the system.

14. Discussion

The data presented above document that the HIC and the later magmatic rocks (dolerite and pegmatite) constitutes a low strain enclave in the WGR. The well-preserved primary features and their progressive reworking allow us to deduce the evolution of this gneiss terrain during the Proterozoic and early Palaeozoic. The 1251 Ma old dolerite dyke intruding the HIC complex with its coronitic texture and mineralogy is identical to dolerites outcropping elsewhere in the WGR, except for its well preserved dyke form. In the rest of the WGR, where hundreds of dolerites are known, they occur as tectonic lenses in the gneisses and are partly or completely reacted into eclogites. The 1654 Ma old HIC is the best-preserved part of the WGR so far encountered and dated and as such it represents a close analogue of the protoliths for much of the gneisses surrounding dolerite lenses elsewhere in the WGR. The Dråga gneiss (Bryhni et al., 1988), for example, displays the same geochemical characteristics as the Hustad complex. Moreover we observe a strong resemblance between the major and trace element data of the pyroxenites, with their high MgO contents, and the eucritic orthopyroxene eclogite in the area, as given by Carswell and Harvey (1985).

The preservation in felsic parts of the complex of Rb–Sr whole rock ages that overlap with the U–Pb ages suggests that changes in Rb, an element generally regarded as mobile during metamorphism, must have been limited in those lithologies. It is, therefore, believed that the observed geochemical signature reflects primary magmatic processes and that this represents a calc-alkaline intrusive complex. This is not to say that the chemical system remained completely undisturbed during the metamorphic overprinting. The MSWD values for the Rb–Sr and Sm–Nd regressions are higher than what can be expected from the analytical uncertainty alone, reflecting at least in part geochemical disturbances. Furthermore, the ε_{Nd} versus Sr I.R plot (Figure 13a) displays a trend that is difficult to explain without invoking some changes in the Rb/Sr and Sm/Nd ratios for the mafic parts of the complex. As discussed above we attribute these disturbances to a loss of Rb and LREE in the pyroxenite and xenoliths where the Caledonian influence was most intense, leading for example to the growth of abundant garnet and local scapolite.

The fact that the rocks of HIC (pyroxenite, monzodiorite, quartz-monzonite and granite) share many chemical characteristics like high Cr and MgO contents, and are spatially related, suggests that they are genetically linked. The granite and the monzodiorite also give identical U–Pb ages. Concentric zoning of mesozonal plutons is a common phenomenon and a trend of increasing acidity towards the core is normal for the majority of them (Stephens et al., 1985). A similar concentric zoning may be the result of fractional crystallisation as suggested for the Rogart pluton by Fowler et al. (2001). Thus, we propose that in the HIC a primary magma of monzodioritic composition may have evolved to quartz-monzonite and granite while the pyroxenite represents possible cumulates of this fractionation. Alternatively the various rock types may represent different but coeval magma types formed by partial melting of a complex source region combined with fractionation.

14.1. Early evolution of the WGR

The intrusive age of 1654 ± 1 Ma of the HIC is at the lower end of a spectrum of U–Pb zircon ages between 1686 and 1653 Ma reported by Tucker et al. (1990) from the Kristiansund area to the north, and is slightly older than ages of 1640 ± 2 and 1631 ± 9 Ma obtained from the Sunnfjord and Sognefjord areas to the south (Skår, 1998; Table 1 and Fig. 1). This restricted period of magmatic activity, and the available isotopic data, indicate that the WGR is largely a juvenile terrain formed rapidly during the Gothian orogeny as already claimed by Gorbatschev (1980) and Skår (2000). The results also suggest that the

WGR is younging southward as proposed by Gorbatschev (1980).

Although many authors have related granitoid rocks to tectonic setting, this remains a subject of controversy and the application of modern plate tectonic concepts to Proterozoic rocks adds an extra degree of uncertainty. Geochemically the HIC classifies as a high-K calc-alkaline to alkalic-calcic suite. The origin and geodynamic setting of such rocks are problematic, but recent workers have suggested that they are predominantly post-collisional (e.g. Liegeois et al., 1998). As pointed out above, the HIC has also many features in common with the late tectonic granites of the British Isles (Harmon et al., 1984), e.g. high Ba and Sr contents and high K_2O relative to SiO_2. The REE pattern and the increasing content of REE from acid to intermediate rocks mimic the features observed in the Strontian, Foyers and Etive complexes (Harmon et al., 1984), although they lack the positive Eu anomalies. Other similarities include the concentric form and size. A major difference is the fact that the late granites of the British Isles show pronounced crustal contamination with negative ε_{Nd} values and very positive ε_{Sr} values (Halliday and Stephens, 1984; Frost and O'Nions, 1985). The HIC is more primitive as brought out by a low Sr I.R. and positive ε_{Nd} values, and in this sense they resemble more the Old Red Sandstone calc-alkaline lavas (Clayburn et al., 1983; Tarney and Jones, 1994), which are associated in terms of age and origin with the late tectonic granites of the British Isles (e.g. the Etive plutonic complex). The Old Red Sandstone-andesites, which share many of the other chemical similarities with the HIC, have a maximal $\varepsilon_{Nd\ (at\ 410\ Ma)}$ of +6 (Thirlwall, 1982). Calculated back to 1654 this will correspond to the maximum values observed in the HIC.

According to Tarney and Jones (1994) the high–K calc-alkaline granites formed dominantly from material melted by thermal pulses in the mantle. We propose a similar interpretation suggesting that the HIC formed in a subduction environment and contains a high proportion of mantle-derived material. In common with modern arc plutons and lavas the HIC shows enrichment in hydrophilic elements (Cs, K, Rb, Sr, Ba) relative to HFSE and REE. This effect cannot be produced by fractional crystallisation of minor REE- and HFSE-rich phases and must have been inherited from a LILE enriched source region. Rocks of the HIC are further characterised by high mg-numbers, and relatively high Cr, Ni and LIL contents. It is to be noted that Skår (2000) describes gneisses with a high-K calc-alkaline signature from southern sectors of the region suggesting that that part of the WGR grew by accretion of island arcs, an interpretation that we can also extend to central and northern parts of the WGR.

Gorbatschev (1980) suggested that the WGR can be correlated with the Southwestern Scandinavian Gneiss Complex (SSGC) of Sweden. The segment of the SSGC that lies east of the Mylonite Zone contains granitoid rocks that resemble the HIC in age, isotope signature (low Sr I.R and positive E_{Nd} values) and geochemistry (Persson et al., 1995) supporting a possible genetic link with the HIC.

The HIC was intruded by a dolerite dyke at 1251 ± 3 Ma. According to Gorbatschev et al. (1987) period of intense dyke formation in the Baltic shield coincides with the earliest events of the Sveconorwegian–Grenvillian orogeny (1250–900 Ma). Dolerites dykes are known from several places in the WGR. Mørk and Mearns (1986) dated dolerites from Flemsøy, Nordøyane, WGR to 1289 ± 48, 1198 ± 56 and 926 ± 70 Ma by Sm–Nd. Dolerites from the Kongsberg sector were also intruded at 1224 ± 15 Ma (Munz and Morvik, 1991) suggesting that the WGR can be linked to the eastern basement sectors below the Caledonian Nappe cover. No Sveconorwegian metamorphic activity is recorded in the Hustad region by the isotope systems studied, in accordance with the U–Pb results on titanite of Tucker et al. (1986/1987). This contrasts with the Sognefjord region (Skår, 1998) and the Lindås and related nappes (Bingen et al., 2001) which locally underwent Sveconorwegian intrusive migmatisation and granulite facies metamorphism.

14.2. The Caledonian evolution

The intrusive age of 401 ± 1 Ma of the pegmatite in the HIC overlaps with the lower intercept age

defined by U–Pb titanite data from the northern WGR (Tucker et al., 1986/1987). These titanite data display various degrees of discordance for different intrusions but they plot all together on a single discordia line with intersections at 396±5 and 1659±2 Ma. From these data Tucker et al. (1986/1987) inferred that the Caledonian influence in the region was short lived and that no thermal event affected the region in the intervening period between 1650 and 396 Ma. In the HIC, besides the 401 Ma age we have also obtained an age of 390 Ma for monazite, which suggests that there was some activity in the area after 400 Ma. The lower intercept age of 384±9 Ma obtained from the dolerite in the HIC probably reflects the same events. The textural relationships in the dolerites, where zircons have developed in fractures in ilmenite, suggest that we have dated a fluid and fracturing event in the area, but it is still unclear whether this fracturing and fluid activity occurred during the main high-pressure event in the area, or whether this event represents the general post-collisional activity which involved large amounts of extension and exhumation to restore the isostatic balance in the crust (Andersen, 1998).

15. Conclusions

The HIC, a concentric pluton ranging in composition from granite to pyroxenite, represents an enclave that has escaped the intense deformation that affected most of the WGR. The complex was formed at a destructive plate margin setting during the Gothian orogeny at 1654±1 Ma, probably by melting of enriched mantle lithosphere and subsequent fractionation of monzodioritic magmas. It was intruded by a dolerite dyke at 1251±3 Ma and was locally metamorphosed and intruded by pegmatites at 401±1 Ma during the Caledonian orogeny. Complexes such as the HIC are likely precursors to many of the gneisses and eclogites of the WGR, which formed within a limited time interval of approximately 40 million years. The Caledonian high pressure metamorphism led to partial-and in shear zones to complete-reaction of the igneous to metamorphic assemblages. In the HIC, the primary magmatic mineralogy and chemical composition are generally well preserved and the felsic members of the complex yield remarkably well behaved Rb–Sr and Sm–Nd systematics that have only marginally been perturbed by the metamorphic overprints. More severe mineralogical and isotopic effects seem to be recorded instead in mafic lithologies, which yield higher Sr and lower Nd initial ratios than the associated felsic units. Although a primary origin of these isotopic characteristics cannot be totally excluded, the bulk of the evidence suggests that they were caused by loss of Rb and of LREE during the fluid-induced metamorphic reactions that formed garnet and scapolite in Caledonian time.

Acknowledgements

The Geological Survey of Norway generously provided the XRF major and trace element data used in this work. We are grateful to Euan W. Mearns and Arne Stabel for skilful help with the Sm–Nd and Rb–Sr isotope work and to Alexander Kühn and Mats Lund for help with some of the illustrations. Constructive reviews by Ø. Nordgulen and Ø. Skår are gratefully acknowledged.

References

Andersen, T.B., 1998. Extensional tectonics in southern Norway, an overview. Tectonophysics 285, 333–351.

Andersen, T.B., Jamtveit, B., Dewey, J.F., Swensson, E., 1991. Subduction and eduction of continental crust: major mechanisms during continent–continent collision and orogenic collapse, a model based on the south Caledonides. Terra Nova 3, 303–310.

Andersen, T., Sundvoll, B., 1995. Neodymium isotope systematics of the mantle beneath the Baltic shield: evidence for depleted mantle evolution since the Archaean. Lithos 35, 235–243.

Austrheim, H., Mørk, M.B.E., 1988. The lower continental crust in continent–continent collision zones; evidence from former deep-seated sections in Western Norway. Norsk Geol. Unders. Spec. Publ. 3, 102–113.

Bateman, P.C., Chappell, B.W., 1979. Crystallization, fractionation, and solidification of the Toulumne Intrusive Series, Yosemite National Park, California. Geol. Soc. Am. Bull. 90, 465–482.

Bingen, B., Austrheim, H., Whitehouse, M., 2001. Ilmenite as a source for zirconium during high-grade metamorphism? Textural evidence from the Caledonides of western Norway and implications for zircon geochronology. J. Petrol. 42, 355–375.

Brown, G.C., 1982. Calc-alkaline intrusive rocks: their diversity, evolution, and relation to volcanic arcs. In: Thorpe, R.S. (Ed.), Andesites; Orogenic Andesites and Related Rocks. Wiley, Chichester, pp. 437–461.

Brueckner, H.K., 1977. A crustal origin of eclogites and a mantle origin for garnet peridotites: strontium isotopic evidence from clinopyroxenes. Contrib. Mineral Petrol. 60, 1–15.

Brunfelt, A.O., Roelandts, I., Steiness, E., 1974. Determination of rubidium, caesium, barium and eight rare elements in ultramafic rocks by neutron-activation analysis. Analyst (London) 99, 277–284.

Bryhni, I., Austrheim, H., Solli, A., 1988. Hustad, 1220 I berggrunnskart 1: 50 000, preliminary map, Nor. Geol. Unders.

Carmichael, I.S.E., 1964. The petrology of Tingmuli, a Tertiary volcano in eastern Iceland. J. Petrol 5, 435–460.

Carswell, D.A., Harvey, M.A., 1985. The intrusive history and tectonometamorphic evolution of the Basal Gneiss Complex in the Moldefjord area, west Norway. In: Sturt, B.A., Gee, D.G. (Eds.), The Caledonian Orogen: Scandinavia and Related Areas. Wiley, New York, pp. 843–857.

Chopin, C., 1984. Coesite and pure pyrope in the high-grade blueschist of the Western Alps: a first record and some consequences. Contrib. Mineral Petrol. 86, 107–118.

Clayburn, J.A.P., Harmon, R.S., Pankhurst, R.J., Brown, J.F., 1983. Sr, O, and Pb isotope evidence for the origin and evolution of the etive igneous complex, Scotland. Nature 303, 492–497.

Corfu, F., Evins, P.M., 2002. Late Palaeoproterozoic monazite and titanite U–Pb ages in the Archean Suomujärvi Complex, N-Finland. Precambrian Res. 116, 171–181.

Crowley, J.L., Ghent, E.D., 1999. An electron microprobe study of the U–Th–Pb systematics of metamorphosed monazite: the role of Pb diffusion versus overgrowth and recrystallization. Chem. Geol. 157, 285–302.

Davidson, A., van Breemen, O., 1988. Baddeleyite-zircon relationships in coronitic metagabbro, Grenville Province, Ontario: implications for geochronology. Contrib. Mineral. Petrol. 100, 291–299.

Dobrzhinetskaya, L.F., Eide, E.A., Larsen, R.B., Sturt, B.A., Trønnes, R., Smith, D.C., Taylor, W.R., Pusukhova, T.V., 1995. Microdiamond in high-grade metamorphic rocks of the Western Gneiss Region, Norway. Geology 7, 597–600.

Fortey, N.J., Cooper, A.H., Henney, P.J., Colman, T., Nacarrow, P.H.A., 1994. Appinitic intrusions in the English Lake district. Mineral. Petrol. 51, 355–375.

Fowler, M.B., Henney, P.J., 1996. Mixed Caledonian appinite magmas: implications for lamprophyre fractionation and high Ba–Sr-granite genesis. Contrib. Mineral. Petrol. 126, 199–215.

Fowler, M.B., Henney, P.J., Darbyshire, D.P.F., Greenwood, P.B., 2001. Petrogenesis of high Ba–Sr granites: the Rogart pluton, Sutherland. J. Geol. Soc. London 158, 521–534.

Frost, C.D., O'Nions, R.K., 1985. Caledonian magma genesis and the crustal recycling. J. Petrol. 26, 515–544.

Frost, B.R., Barnes, C.G., Collins, W.J., Arculus, R.J., Ellis, D.J., Frost, C.D., 2001. A geochemical classification for granitic rocks. J. Petrol. 42, 2033–2048.

Gorbatschev, R., 1980. The Precambrian development of southern Sweden. GFF 102, 129–136.

Gorbatschev, R., Gaal, G., 1987. The precambrian history of the Baltic Shield. In: Kröner, A. (Ed.), Proterozoic Lithospheric Evolution, vol. 17. AGU-CSA Geodynamic series, pp. 149–159.

Gorbatschev, R., Lindh, A., Solyom, Z., Laitakari, I., Aro, K., Lobach-Zhuchenko, S.B., Markov, M.S., Ivliev, A.I., Bryhni, I., 1987. Mafic dyke swarms of the Baltic Shield. Geol. Ass. Can. Spec. Pap. 34, 361–372.

Griffin, W.L., Brueckner, H.K., 1985. REE, Rb–Sr and Sm–Nd studies of Norwegian eclogites. Chem. Geol. 52, 249–271.

Groome, D.R., Hall, M.A., 1974. The geochemistry of the Devonian lavas of northern Lorne Plateau, Scotland. Min. Mag. 39, 621–640.

Halliday, A.N., Stephens, W.E., 1984. Crustal controls on the genesis of the 400 Ma old Caledonian granites. Phys. Earth Planet Interiors 35, 89–104.

Heaman, L.M., LeCheminant, A.N., 1993. Paragenesis and U–Pb systematics of baddeleyite (ZrO_2). Chem. Geol. 110, 95–126.

Harmon, R.S., Halliday, A.N., Clayburn, J.A.P., Stephens, W.E., 1984. Chemical and isotopic systematics of the Caledonian intrusions of Scotland and Northern England: a guide to magma source region and magma-crust interaction. Phil. Trans. R. Soc. London A 310, 709–742.

Hernes, I., 1956. Eclogite-amphibolite on the Molde peninsula, Southern Norway. Norsk Geol. Tidsskr. 33, 163–184.

Hofmann, A.W., 1988. Chemical differentiation of the Earth: the relationship between mantle, continental crust, and oceanic crust. Earth Planet Sci. Lett. 90, 297–314.

Krogh, T.E., 1973. A low contamination method for hydrothermal decomposition of zircon and extraction of U–Pb for isotopic age determinations. Geochim. Cosmochim. Acta 37, 485–494.

Krogh, E.J., 1977. Evidence for a precambrian continent–continent collision in western Norway. Nature 267, 17–19.

Krogh, T.E., 1982. Improved accuracy of U–Pb zircon ages by the creation of more concordant systems using an air abrasion technique. Geochim. Cosmochim. Acta 46, 637–649.

Krogh, E.J., Brunfelt, A.O., 1981. REE, Cs, Rb, Sr and Ba in glaucophane-bearing eclogites and associated rocks, Sunnfjord, Western Norway. Chem. Geol. 33, 295–305.

Lappin, M.A., Pidgeon, R.T., van Breemen, O., 1979. Geochronology of basal gneisses and mangerite syenites of Statlandet, west Norway. Norsk Geol. Tidsskr. 59, 161–181.

Larsen, E.S., 1948. Batholith and associated rocks of Corona, Elsinore and San Luis Rey Quadrangles southern California. Mem. Geol. Soc. Am. 29, 182.

Liegeois, J.-P., Navez, J., Hertogen, J., Black, R., 1998. Contrasting origin of post-collisional high-K calc-alkaline and shoshonitic versus alkaline and peralkaline granitoids; the use of sliding normalization. Lithos 45, 1–28.

Ludwig, K.R., 1999. ISOPLOT/EX version 2.03. A geochronological toolkit for MICROSOFT excel, Berkeley Geochron. Center. Spec. Publ. 1, 43.

Mearns, E.W., 1986. Sm–Nd ages for Norwegian garnet peridotites. Lithos 19, 269–278.

Mørk, M.B.E., 1985. Incomplete high P-T metamorphic transitions within the Kvamsøy pyroxenite complex, west Norway: a case study of disequilibrium. J. Metam. Geol. 3, 245–264.

Mørk, M.B.E., Mearns, E.W., 1986. Sm–Nd isotopic systematics of a gabbro-eclogite transition. Lithos 19, 255–267.

Munz, I.A., Morvik, R., 1991. Metagabbros in the Modum Complex, southernNorway: an important heat source for the Sveconorwegian metamorphism. Precambrian Res. 52, 97–113.

Peacock, M.A., 1931. Classification of igneous rock series. J. Geol. 39, 54–67.

Peccerillo, A., Taylor, S.R., 1976. Geochemistry of Eocene calc-alkaline volcanic rocks from the Kastamona area, northern Turkey. Contrib. Mineral. Petrol. 58, 63–81.

Persson, P.-O., Lindh, A., Schønberg, H., Hansen, B.T., Lagerblad, B., 1995. A comparison of the geochronology and geochemistry of the plagioclase-dominated granitoids across a major terrane boundary in the SW Baltic Shield. Precambrian Res. 74, 57–72.

Prince, C., Harris, N., Vance, D., 2001. Fluid-enhanced melting during prograde metamorphism. J. Geol. Soc. London 158, 233–241.

Schnetzler, C.C., Philpotts, J.A., 1970. Partition coefficients of rare-earth elements between igneous matrix and rock-forming mineral phenocrysts—II. Geochim. Cosmochim. Acta 34, 331–340.

Skår, Ø., 1998. Field relations and geochemical evolution of the pre-Sveconorwegian rocks in the Kvamsøy area, southern Western Gneiss Complex, Norway. In: Skår, The Proterozoic and early Paleozoic evolution of the southern parts of the Western Gneiss Complex. Unpublished Ph.D. Thesis, University of Bergen.

Skår, Ø., 2000. Field relations and geochemical evolution of the Gothian rocks in the Kvamsøy area, southern Western Gneiss Complex, Norway. Nor. Geol. Unders. Bull. 437, 5–23.

Skår, Ø., Pedersen, R.B., 1998. Relations between granitoid magmatism and migmatization: U–Pb geochronological evidences from the Western Gneiss Complex, Norway. In: Skår, The Proterozoic and early Paleozoic evolution of the southern parts of the Western Gneiss Complex. Unpublished Ph.D. thesis, University of Bergen.

Skår, Ø., Furnes, H., Claesson, S., 1994. Middle proterozoic magmatism within the Western Gneiss Region, Sunnfjord, Norway. Norsk Geol. Tidsskr. 74, 114–126.

Smith, I.E., 1972. High-potassium intrusives from south eastern Papua. Contrib. Mineral. Petrol. 34, 167–176.

Smith, D.C., 1984. Coesite in clinopyroxene in the Caledonides and its implication for geodynamics. Nature 310, 641–644.

Stacey, J.S., Kramers, J.D., 1975. Approximation of terrestrial lead isotope evolution by a two-stage model. Earth Planet Sci. Lett. 34, 207–226.

Stephens, W.E., Whitley, J.E., Thirlwall, M.F., Halliday, A.N., 1985. The Criffell zoned pluton: correlated behaviour of rare earth element abundances with isotopic systems. Contrib. Mineral. Petrol. 89, 226–238.

Tarney, J., Jones, C.E., 1994. Trace element geochemistry of orogenic igneous rocks and the crustal growth models. J. Geol. Soc. London 151, 855–868.

Taylor, S.R., McLennan, S.M., 1985. The Continental Crust: its Composition and Evolution: An Examination of the Geochemical Record Preserved in Sedimentary Rocks. Blackwell Science Publishers, Oxford, p. 312.

Thirlwall, M.F., 1982. Systematic variation in chemistry and Nd–Sr isotopes across a Caledonian calc-alkaline volcanic arc: implications for source materials. Earth Planet Sci. Lett. 58, 27–50.

Tucker, R.D., Råheim, A., Krogh, T.E., Corfu, F., 1986. Uranium-lead zircon and titanite ages from the northern portion of the Western Gneiss Region, south-central Norway. Earth Planet Sci. Lett. 81, 203–211.

Tucker, R.D., Krogh, T.E., Råheim, A., 1990. Proterozoic evolution and age-province boundaries in the central part of the Western Gneiss Region, Norway: results of U–Pb dating of accessory minerals from Trondheimsfjord to Geiranger. In: Gower, C.F., Rivers, T., Ryan, B. (Eds.), Mid-Proterozoic geology of the Southern Margin of Proto-Laurentia-Baltica. Geol. Assoc. Can. Spec. Pap. 241 pp. 33–50.